AN EXPERIMENTAL AND THEORETICAL INVESTIGATION OF TWO-DIMENSIONAL CENTRIFUGAL PUMP IMPELLERS

Thesis by

Allan James Acosta

In Partial Fulfillment of the Requirements

For the Degree of

Doctor of Philosophy

California Institute of Technology

Pasadena, California

1952

ABSTRACT

An experimental and theoretical investigation on a series of three centrifugal pump impellers has been made in order to determine the usefulness and validity of two-dimensional potential theory for the description of the flow. Computed values of the developed head and distribution of pressure on the vane surfaces are compared with measurements on two-, four-, and six- bladed impellers which have 30° logarithmic spiral vanes and a radius ratio of about one-half.

It is found that for operating points where the influence on the flow into the impeller by the inlet turn is least, the agreement between the observed and predicted values is reasonably good, while for other flow rates large discrepancies occur. Although the impeller efficiency is relatively high when the flow is least disturbed by the inlet, the slope of the work coefficient line is steeper than the theoretically predicted value. This deviation is attributed to boundary layers which are observed on the vane surfaces.

ACKNOWLEDGMENTS

The writer would like to express his indebtedness to Professors A. Hollander, M. S. Plesset, and W. D. Rannie for their many suggestions and continued interest in this work. The support given by Mr. John B. Keating and the Office of Naval Research is also gratefully acknowledged.

TABLE OF CONTENTS

I. INTRODUCTION

In the past most of the experimental work in the field of hydraulic machinery has been conducted on complete machines. Because of the mechanical difficulties involved, relatively little work has been done to determine the performance and behavior of the individual components. Roughly, a hydraulic machine may be considered to be composed of three parts; a stationary inlet or guide device, a rotating component or impeller, and volute or stationary collecting device.

With a view to obtaining component performances, much experimental work has been done in testing combinations of impellers in various volutes. Individual performance is then inferred from changes in over-all behavior. A separate study of the components permits a more ready understanding of the processes occurring and through simplification allows analysis to be undertaken. If the complete characteristics of the individual elements of the machine were then either known or predictable, design would become more straightforward.

Since the impeller is responsible for energy input to the flow, it seems clear that it should be the item of first interest. It would be highly desirable to be able to predict the head developed and the distributions of pressure which occur by methods other than the empirical cut and try. However, a satisfactory theory embracing all of the effects of real fluids and the complex geometries found in practice is not yet available. For that reason the problem must be simplified as far as possible retaining only the essentials. To this end the impeller is assumed to be two dimensional, that is, the flow is restricted to depend only on radial and angular coordinates. For analysis, it is further assumed to be inviscid, incompressible and irrotational so that the methods of potential theory

may be employed.

This approach is familiar in fluid mechanics and much success has been obtained with it. However, it should be noted at the outset that the limitations of potential theory for flows of the sort described above are as yet unknown.

The line of thought followed in this work is not novel. It is to be found in references (1) to (3) to mention a few of the current efforts. However, in most of these works the configurations studied are such that analysis or comparison with a theory in any systematic way is difficult.

II. THEORETICAL TREATMENT

In this section the solution for the potential flow due to a rotating array of logarithmic spiral blades is outlined. The flow is assumed to be two dimensional, thus permitting application of complex variable theory. This problem has been previously treated by a number of writers [4], [5] who only determined the relation between the head developed and the flow rate in addition to the flow rate for "shockless" entrance, i.e., that flow rate for which the entering flow streams smoothly onto the blade leading edge. Blade pressure distributions have been calculated for straight radial blades for one and two blades[6] and for a few specialized cases by an approximate procedure[7]. In the following paragraphs the development outlined follows that of Ref. (4).

The velocity field due to a rotating impeller (see Fig. 1) may be resolved into two components; namely, (a) that resulting from rotation of the vanes in still fluid designated as the "displacement" flow, and (b) the component due to a line source placed at the origin of a stationary

vane system. This latter solution corresponds to pure "through flow" with no rotation and accounts for net discharge of the impeller. Various operating conditions then may be obtained by a linear combination of solutions (a) and (b). This procedure is validated by the linearity of Laplace's equation and the fact that each solution separately satisfies its own boundary condition. In order to effect a solution of these boundary value problems, a conformal mapping is employed which transforms the physical given plane into one in which the circular system of blades is mapped onto a circle.

The Mapping Function

The conformal mapping employed is due originally to Konig (Ref. 8) although it is presented here in slightly different form. The function is (Fig. 1)

$$Z = \left[\frac{w_0 - w}{w_0 - 1}\right]^{\frac{1}{N}} \left[\frac{w_0 - \frac{1}{w}}{\overline{w}_0 - 1}\right]^{\frac{e^{2i\gamma}}{N}} , \qquad (1)$$

and

$$\frac{dZ}{Z} = \frac{e^{i\gamma}}{N} \cdot \frac{dw}{w}\left[\frac{\frac{e^{i\gamma}}{w}}{\overline{w}_0 - \frac{1}{w}} - \frac{e^{-i\gamma} w}{w_0 - w}\right] , \qquad (2)$$

where Z and w are the physical and circle planes respectively. N is the number of blades and $\frac{\pi}{2} - \gamma$ is the vane angle. This function maps the system of N vanes onto the unit circle in the w plane in such a way that the region exterior to the unit circle is mapped onto the Z plane. The complex constant w_0 corresponds to the origin in the Z plane and its value depends on the various geometrical parameters of the impeller. That Eq.(1) represents the required mapping is easily verified since on the unit circle Eq. (2) gives $\arg(dZ/Z) = \gamma$ when $w = e^{i\theta}$. This result is precisely the requirement for a logarithmic spiral. Equation (1)

is an N valued function (N integral) such that if the point w_o is encircled once in a counterclockwise direction then arg Z increases by $2\pi/N$. In this way congruent points in each of the N passages of the impeller are mapped onto the circle plane in a one-to-one manner.

The singular points of the mapping are given by the roots of $\frac{dZ}{dw}=0$, and they determine the end points of the logarithmic spirals. Setting Eq. (2) equal to zero, one finds these points from the solution of the quadratic equation:

$$e^{2i\gamma}\left[w_o - w\right] = \bar{w}_o w^2 - w \quad .$$

If the two solutions are denoted by w_1 and w_2, one has

$$w_1 + w_2 = \frac{1 - e^{2i\gamma}}{\bar{w}_o}$$

$$w_1 w_2 = -e^{2i\gamma}\frac{w_o}{\bar{w}_o} \quad .$$

For convenience the point $w = 1$, representing the blade tip, is chosen as w_2 giving then for w_1,

$$w_1 = e^{i(2\gamma + 2\delta + \pi)} \tag{3}$$

in which $w_o = a e^{i\delta}$.

From the foregoing relations, a is found to be

$$a = \frac{\sin\gamma}{\sin(\gamma+\delta)} \quad . \tag{4}$$

The tip radius corresponds to $r_2 = |Z_2| = 1$, so that the ratio of inlet to outlet radius is given by $|Z_1|$, i.e.,

$$\frac{r_1}{r_2} = |Z| = \left| \left[\frac{w_o - w_1}{w_o - 1}\right]^{\frac{1}{N}} \cdot \left[\frac{\bar{w}_o - \frac{1}{w_1}}{\bar{w}_o - 1}\right]^{\frac{e^{2i\gamma}}{N}} \right| ,$$

or

$$\frac{r_1}{r_2} = \left[\frac{w_0 - w_1}{w_0 - 1}\right]^{\frac{1}{N}} \cdot \left[\frac{\bar{w}_0 - \frac{1}{\bar{w}_1}}{\bar{w}_0 - 1}\right]^{\frac{1+\cos 2\gamma}{N}} \cdot e^{-\frac{\sin 2\gamma}{N} \arg \frac{w_0 - 1}{w_0 - w_1}}$$

which becomes after suitable reduction:

$$\frac{r_1}{r_2} = \left[-\frac{\sin(2\gamma+\delta)}{\sin\delta}\right]^{\frac{1+\cos 2\gamma}{N}} \cdot e^{-\frac{2(\pi-\delta-\gamma)}{N} \sin 2\gamma} \quad . \qquad (5)$$

It should be noted from Fig. 1 that $2\gamma + \delta \geqq \pi$. If r_1/r_2, N and γ are given, α and δ may be found from Eqs. (4) and (5).

There are two contributions to the flow potential in the w plane: (a) the displacement flow resulting from rotation of the blades, (b) the through flow resulting from a source at the origin (in the Z plane) with the blades stationary. For the establishment of lift on the blade, the Kutta condition which requires finite velocity at the vane trailing edges is imposed on each of the above flows.

a. <u>The Displacement Flow</u>

The boundary condition at a solid surface requires that there is no flow through the surface. Upon reference to the sketch below it is readily seen that this condition is fulfilled if

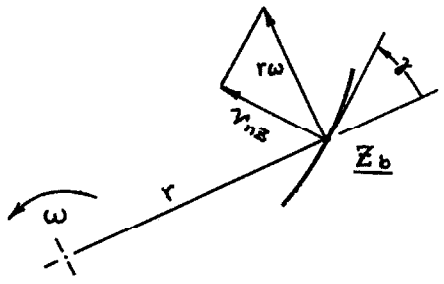

$$v_{nZ} = \omega \cos\gamma \, Z_b \, e^{i(\frac{\pi}{2}+\gamma)} \quad .$$

Let F be the complex potential for the flow; then

$$\frac{dF}{d\omega} = \frac{dF}{dZ} \cdot \frac{dZ}{d\omega} \quad ,$$

$$\frac{dF}{d\omega} = V_{nZ} \frac{dZ}{d\omega} \quad .$$

V_{nZ} is the conjugate of the vector velocity $\mathcal{V}_{nZ}$. Since polar coordinates are employed in the ω plane, the boundary condition is expressed there as

$$V_{r\omega} e^{-i\theta} = \omega \cos\gamma \, \overline{Z}_b \frac{dZ_b}{d\omega} e^{-i(\frac{\pi}{2}+\gamma)} \tag{6}$$

in which subscript " b " refers to the blade. The substitution $\omega = e^{i\theta}$ in Eq. (6) gives

$$V_{r\omega} = -i \frac{\omega \cos\gamma}{N} Z_b \overline{Z}_b \left[\frac{e^{i(\gamma-\theta)}}{\overline{\omega}_o - e^{-i\theta}} - \frac{e^{i(\gamma-\theta)}}{\omega_o - e^{i\theta}} \right]$$

as the boundary condition for the radial velocity in the ω plane.

The quantity $Z_b \overline{Z}_b$ may be found from Eq. (1) so that the boundary condition in the ω plane is expressed as

$$V_{r\omega} = -i \frac{\omega \cos\gamma}{N} \left[\frac{\omega_o - e^{i\theta}}{\omega_o - 1} \right]^{\bar{q}} \left[\frac{\overline{\omega}_o - e^{-i\theta}}{\overline{\omega}_o - 1} \right]^{q} \left[\frac{e^{i(\gamma-\theta)}}{\overline{\omega}_o - e^{-i\theta}} - \frac{e^{i(\gamma-\theta)}}{\omega_o - e^{i\theta}} \right] \quad , \tag{7}$$

where $q = \frac{1}{N}\left[1 + e^{2i\gamma}\right]$.

In addition to the boundary condition on the blade, there is the further requirement that the velocity vanish at infinity in both planes since it is assumed that there will be no disturbance there. With these stipulations the complex potential representing the flow may be written in the form of a Laurent series

$$F(w) = \sum_{n=0}^{\infty} a_n w^{-n}$$

and the coefficients a_n may be determined from Eq. (7) on the unit circle. The velocity field can then be found by differentiation of this series. For cases of practical interest, the function represented by Eq. (7) has a single, very sharp peak with the result that a large number of the coefficients a_n are required. In this work, the items of principal interest are the head generated and the pressure distribution on the blades. For the determination of these quantities it is necessary to obtain only the tangential velocity component on the unit circle corresponding to the radial component given by Eq. (7) subject to the condition that the velocity vanish at infinity. To obtain the conjugate function directly, a form of Poisson's integral may be used (Ref. 9). Then the tangential velocity on the unit circle in the w plane is given by the integral,

$$V_t(\theta) = -\frac{1}{2\pi}\int_0^{2\pi} V_r(\phi)\cot\frac{\phi-\theta}{2}\,d\phi \qquad (8)$$

If $V_r(\phi)$ is at least piecewise continuous, then the principal value of the above integral provides the required result. For the special cases studied in this work, it was found expedient to approximate $V_r(\phi)$ by a function whose conjugate was known and to apply Eq. (8) to the difference, thus facilitating numerical accuracy and speed.

Substitution of Eq. (7) into Eq. (8) gives for the tangential displacement velocity

$$V_{tw}(\theta) = i\,\frac{\omega\cos\gamma}{2\pi N}\int_0^{2\pi}\left[\frac{w_o - e^{i\phi}}{w_o - 1}\right]^{\bar{\gamma}}\left[\frac{\bar{w}_o - e^{-i\phi}}{\bar{w}_o - 1}\right]^{\gamma}\left[\frac{e^{i(\gamma-\phi)}}{\bar{w}_o - \bar{e}^{i\phi}} - \frac{\bar{e}^{i(\gamma-\phi)}}{w_o - e^{i\phi}}\right]\cot\frac{\phi-\theta}{2}\,d\phi\,. \qquad (9)$$

From Fig. 1 it is evident that the point $w = 1$ maps into the blade trailing edge. The requirement of finite velocity there means that

$$V_t \Big)_{\theta=0} = 0 \ .$$

This condition may be satisfied without disturbing the boundary condition of Eq. (7) by introducing a vortex at the origin in the w plane of such strength that

$$V_t \Big)_{\theta=0} + \frac{\Gamma}{2\pi} = 0 \ .$$

The value of $V_t \Big)_{\theta=0}$ is given the special notation V_{a2} . The tangential displacement velocity on the unit circle satisfying Kutta's condition at the exit tip is thus

$$V_{twa} = V_{tw} + V_{a2} \tag{10}$$

with a circulation of strength $\Gamma_a = -2\pi V_{a2}$ (the subscript "a" refers to the displacement flow.)

b. The Through Flow

To obtain the effect of net discharge from the impeller, the vane system is regarded as being stationary and the flow resulting from a line source at the origin in the Z plane is determined. As in section (a), it is necessary to determine only the tangential velocities on the unit circle although this constitutes no real restriction in evaluating the flow.

The point w_o is mapped by Eq. (1) into the origin in the physical plane. To determine the complete through-flow potential, the flow about the unit circle due to a source at w_o must be obtained. The required potential is readily found by the method of images to be

$$G(w) = \frac{Q}{2\pi} \log(w - w_o) + \frac{Q}{2\pi} \log\left(\frac{1}{w} - w_o\right) \qquad (11)$$

where Q is the (complex) source strength in the w plane. As yet no requirement has been put on Q. If Q is complex, then the flow in the Z plane issues from the origin on logarithmic spirals with an angle $\arg Q$ between the spiral and any radius. Thus, the effect of inlet guide vanes may be approximated by a suitable complex value of Q. Such "prerotation" has been observed on complete pumping installations in the inlet pipe (Ref. 10), although observations on free impellers (Ref. 11) indicate little or no prerotation. For free, two-dimensional impellers there is no reason for prerotation to exist, and since these calculations are to be compared to experiments conducted on free impellers, Q is assumed to be real throughout the rest of this work. The velocity components are found by differentiation of Eq. (11), and on the unit circle they are;

$$V_r = 0$$

$$V_t = \frac{Q\, a \sin(\theta - \delta)}{\pi\left[1 + a^2 - 2a\cos(\theta - \delta)\right]} \quad , \qquad (12)$$

and

$$V_t\Big)_{\theta=a} = V_{b2} = -\frac{Q\, a \sin\delta}{\pi\left[1 + a^2 - 2a\cos\delta\right]} \quad . \qquad (12a)$$

The through flow must also satisfy Kutta's condition at the exit tip. As in (a), the addition of a simple vortex at the origin satisfies this condition if its strength is adjusted to give zero velocity at $w = 1$.

Hence,

$$\frac{\Gamma_b}{2\pi} = -V_{b2} \quad ,$$

or

$$\frac{\Gamma_b}{2\pi} = \frac{Q\,a\sin\delta}{\pi\left[1+a^2-2a\cos\delta\right]} \quad . \tag{13}$$

The total tangential through flow velocity is thus,

$$V_{twb} = \frac{aQ}{\pi}\left[\frac{\sin(\theta-\delta)}{1+a^2-2a\cos(\theta-\delta)} + \frac{\sin\delta}{1+a^2-2a\cos\delta}\right] \quad . \tag{14}$$

Equations (1), (9), (10), and (14) constitute the required solution of the potential flow for a two-dimensional rotating pump impeller with equally spaced logarithmic spiral blades. Any operating condition may be obtained by a linear combination of V_{twa} and V_{twb} . The head vs. flow rate diagram is yet to be determined, and the condition for shockless entrance, i.e., the flow rate for which the velocity at the inlet tip is finite.

The Developed Head

The head developed by the impeller is

$$H = \frac{1}{g}\left[u_2\overline{c_{u_2}} - u_1\overline{c_{u_1}}\right]$$

where u_1 , u_2 are inner and outer tip speeds, respectively, and $\overline{c_{u_1}}$, $\overline{c_{u_2}}$ are the average values of the tangential component of the absolute velocity in the direction of rotation. As in (b), prerotation is presumed to be zero, hence $\overline{c_{u_1}} = 0$. If Γ_z designates the value of the circulation in the z plane measured positive counterclockwise, then

$$\psi = \frac{H}{U_2^2/g} = \frac{\Gamma_z}{2\pi r_2 u_2} \tag{15}$$

where ψ is a dimensionless head coefficient. A circuit once in the positive (counterclockwise) direction about the unit circle in the plane corresponds to a circuit in the positive direction around one impeller vane. The total circulation in the plane is thus equal to N times the circulation about one blade. Thus, if

$$\Gamma_w = \Gamma_a + \Gamma_b$$

is the circulation in the w plane, then

$$\Gamma_z = N\left[\Gamma_a + \Gamma_b\right] \tag{16}$$

The dimensionless head coefficient ψ is

$$\psi = \frac{1}{2\pi r_2 u_2}\left[N\Gamma_a + N\Gamma_b\right] \quad ,$$

or

$$\psi = \frac{NV_{a2}}{r_2 u_2} + \frac{NV_{b2}}{r_2 u_2} \quad .$$

The first term is dependent only on the rotation of the blades and the second is a function only of the flow rate. The dimensionless quantity $NV_{a2}/r_2 u_2$ is incorporated into the single constant ψ_o which is otherwise known as the shut-off head. According to Eq. (12a), one has

$$\frac{NV_{b2}}{r_2 u_2} = \frac{NQ\,a\sin\delta}{r_2 u_2 \pi\left[1 + a^2 - 2a\cos\delta\right]} \quad ,$$

where Q is the flow rate in the w plane and consequently represents

the flow rate per passage in the physical plane. (Q is the flow rate per unit width and hereafter it and all coefficients derived from it mean per unit width.) A flow-rate coefficient may be defined as

$$\phi = \frac{C_{m2}}{u_2} = \frac{Q}{A_2 u_2}$$

where now Q is the total flow rate of the impeller. Thus,

$$\phi = \frac{NQ}{2\pi r_2 u_2} \quad , \tag{17}$$

and

$$\psi = \psi_o + \phi \frac{2a \sin\delta}{1 + a^2 - 2a\cos\delta} \quad .$$

It is convenient to express the factor of ϕ in this relation as a multiple of tan γ, that is,

$$\psi = \psi_o + C_v \phi \tan\gamma \tag{18}$$

in which

$$C_v = \frac{2a \sin\delta}{1 + a^2 - 2a\cos\delta} \cdot \frac{1}{\tan\gamma} \quad . \tag{19}$$

Equation (18) is the required relation between the head developed and the flow rate. If the number of blades $N \longrightarrow \infty$, then $\psi_o, C_v \longrightarrow 1$ so that

$$\psi = 1 + \phi \tan\gamma$$

This expression is the so-called Euler head since it was first determined by him by assuming that the vanes perfectly guided the fluid. The constant ψ_o expresses the effectiveness of the blades in bringing up the absolute flow to a tip speed of $u_2 = r_2\omega$; and the coefficient C_v indicates their effectiveness in making the leaving angle of the through flow

equal to the vane angle.

The values of the coefficients ψ_o, C_v satisfy the inequality

$$0 \leq \psi_o , C_v \leq 1 \quad .$$

Typical values of ψ_o for impeller with moderate numbers of blades (5 to 8), vane angles $\beta = \frac{\pi}{2} - \gamma$ of 20 to 40° are 0.6 to 0.8 if the radius ratio is around one half or less. For these cases C_v is always nearly unity.

Condition of Shockless Entry

Impellers with blades which are backward curved* have a particular flow-rate coefficient for which the velocity at the inlet edge is finite. For an infinite number of vanes this point (denoted by "shockless" entry) is equal to the flow rate at which the entering relative velocity is parallel to the inlet vane section. However, for a finite number of vanes this flow rate must be determined from the condition that the tangential velocity is zero at the point in the circle plane corresponding to the vane inlet tip. This condition is expressed by the equation

$$V_{t\omega a}(\theta_1) + V_{t\omega b}(\theta_1) = 0$$

or

$$V_{t\omega a}\Big|_{\theta = 2\gamma + 2\delta + \pi} + \phi \frac{2a}{N}\left[\frac{\sin(\theta - \delta)}{1 + a^2 - 2a\cos(\theta - \delta)} + C_v \tan\gamma\right]\Bigg|_{\theta = 2\gamma + 2\delta + \pi} = 0 \qquad (20)$$

---

*With reference to Fig. 1, backward curved blades are obtained by letting γ be positive in the direction shown and the rotative speed be $(-\omega)$, or vice versa.

The flow rate and head developed at shockless entry are designated as ϕ_e and ψ_e, respectively.

Pressure and Velocity Distribution

The velocities in the w plane may be transformed to corresponding velocities in the Z plane by the relation

$$\frac{dF}{dZ} = \frac{dF}{dw} \cdot \frac{dw}{dZ}$$

where F is the complex potential for the flow. Let v_{tZ} be the tangential vector velocity on the blade surface in the Z plane. Eq. (6) then gives

$$v_{tZ} = iV_{tw} \frac{v_{nZ}}{V_{rw}} \tag{21}$$

on the blade.

From Fig. (2) it is evident that the relative velocity is

$$W = -r\omega \sin\gamma - v_{tZ} \tag{22}$$

along the blade. Since the relative flow is steady and the absolute flow irrotational, blade pressures may be computed from Eq. (22) by using the Bernoulli equation for rotating coordinates

$$p + \tfrac{1}{2}\rho \left[W^2 - r^2\omega^2\right] = \text{CONST.} \tag{23}$$

In this work the constant is chosen to be the inlet total pressure P_T. A pressure coefficient may then be defined as

$$C_p = \frac{P - P_T}{\frac{1}{2}\rho U_2^2} = \left[\frac{r}{r_2}\right]^2 - \left[\frac{W}{U_2}\right]^2 \tag{24}$$

and by means of Eqs. (22), (21), (14), and (10) values of C_p along the blade may be computed.

Numerical Evaluation and Results

The potential problem outlined above was evaluated for three cases in which $r_1/r_2 = 0.54$, $\beta = \frac{\pi}{2} - \gamma = -30^\circ$ were constants, and N was 2, 4, and 6. Numerical integration of Eq. (9) offered no difficulty for N = 2 and 4; however, the integrand for N = 6 was quite sharp and peaked. For that reason a function whose conjugate was known was subtracted from the integrand and the resulting difference integrated. The numerical procedure of Peebles was used (Ref. 12).* Values of the function were computed at 80 equally spaced points around the unit circle and in the case of N = 6, additional points were found to be necessary in the vicinity of w_1. Again for N = 6, the value of a was very nearly equal to unity. As a consequence, the integrand of Eq. (9) changed rapidly in the vicinity of $\theta = \delta$ which made it difficult to secure an exact value of ϕ_e. From the computations, it is believed that ϕ_e is good to three figures at least whereas the values of ψ_o, C_p should be good to four figures.

Pressure distributions for shockless entrance and various other flow rates were computed for the cases noted above and are plotted in Figs. 3, 4, and 5.

The values of ψ_o and ϕ_e are tabulated in Table I together with comparative values from Ref. (4) and with the results of infinite vane theory.

---

* This method is an 80 point numerical integration of $\int_0^{2\pi} f(\varphi) \cot(\varphi-\theta)/2 \, d\varphi$. Second, third, and higher differences are used to provide corrections for excess curvature in the function $f(\varphi)$.

TABLE I

		ψ_o	φ_e	ψ_e
N = 2	This work	0.38	.31	0.11
	Busemann (Ref. 4)	0.38	.31	0.11
N = 4	This work	0.63	.27	0.24
	Ref. 4	0.66	.29	0.23
N = 6	This work	0.76	.24	0.36
	Ref. 4	0.76	.26	0.35
N = ∞		1.00	.168	0.66

The comparison is excellent for N = 2 while for N = 4, 6 the results differ by a few percent. The reasons for the discrepancy are unknown, for the computation procedure was such as to give at least three figure accuracy, although it is conceivable that an arithmetical error was made, or the graphs of Ref. 4 were incorrectly plotted.

III. EXPERIMENTAL APPARATUS AND EQUIPMENT

Three experimental impellers were constructed and tested in the Rotating Channels test stand of the Hydrodynamics Laboratory. Although this apparatus has been described elsewhere, (Ref. 1) it is appropriate to mention its salient features here.

Essentially, the equipment consists of a reservoir, a pump, and a system of piping to provide a flow of water in a closed circuit. Venturi meters are provided to measure flow of water at various pressures and flow rates. The flow may be distributed to any one of three test basins in either one of two directions. The test basin used for the present work was provided with a 1/2 hp. "V" belt impeller drive. Water was delivered to the impeller via an approach section in which a honeycomb flow-

straightener five diameters upstream had been installed. The impeller discharged into an open tank and led back to the reservoir. A speed control device attached to the impeller drive mechanism maintained the impeller at a constant rpm, measured by a "Strobotac".

The assembled impeller and drive mechanism is shown in Fig. 6 in cross section. A pair of stationary circular plates form an annulus which serves to keep the flow parallel a short distance outside the impeller and provides a convenient mounting for flow survey probes.

The Test Impellers

Three test impellers (Fig. 7) were constructed with the same parameters as those cases theoretically treated, i.e., $r_1/r_2 = 0.54$, $\beta = 30^\circ$; N = 2, 4, and 6. A relatively abrupt simple turn deflects the flow from the axial to radial direction (see Fig. 7). It was impossible to use a vaned turn which would have given more uniform inlet velocities at the impeller entrance, as the setup limitations would have prevented the measurement of the head.. Impeller vanes were made of 1/8" brass sheet bent to the proper logarithmic spiral contour. Corresponding curved slots machined in the lucite shrouds positioned the blades accurately. The resulting assembly was held together by screws tapped into the top and bottom sides of the vanes. The impellers were then turned to 12.000 in. in a lathe leaving the vane tips 1/4 in. wide, which may have some significance in the deviation of theory and experiment. The bottom shroud was jig-drilled to center and to run true on the driving assembly.

Actually only two impellers were fabricated; an 8-vaned one which was later altered to four, and a 6-vaned one which was subsequently dismantled and reassembled with two vanes.

The breadth of the impellers is a nominal one inch. This dimension is about the allowable maximum which does not impose a severe retardation of the average flow around the inlet turn. The resulting low aspect ratio of the passage is typical of impellers with design flow rate coefficients of around 0.10 to 0.15.

Instrumentation

The determination of blade pressure distributions requires the measurement of pressure signals on a rotating device. Customarily such signals are measured with a stationary manometer in conjunction with a complicated system of rotating seals. The complexity of such a device was circumvented by constructing a multi-tube manometer which was rigidly attached to the impeller. The manometer was circular and mounted concentrically with the impeller centerline, and was equipped with twenty-seven 5 mm. glass tubes 18 in. long. The manometer readings were converted into actual pressures by accounting for the relative centrifugal force effects. In this way a complete determination of blade static pressures could be obtained in one setup by observing the tubes with the aid of a synchronized strobolight.

Thirteen piezometer taps 0.030 in. in diameter were installed on opposite sides of two diametrically opposite vanes at the mid-elevation of the passage. The taps communicated with 1/16-in. holes drilled down the height of the vane. Transparent plastic tubing then led off the pressure signal to the rotating manometer.

The reference pressure was chosen to be the inlet total pressure. It was measured by a 3/16-in. simple impact tube located on the impeller center line.

The head developed by the impeller was measured by two stationary

total head probes aligned with the flow. A 1/4-in. simple impact probe mounted on the impeller center line in the throat of the approach section (Fig. 7) measured the inlet total head and a Venturi-type total head probe (kiel No. SKD 700) mounted 1/8 in. from the impeller o.d. was used to survey the average discharge total head. A 2.5-ft. stationary water manometer composed of two 6 mm. glass tubes was used to read these pressures. A small amount of aerosol added to the fluid of both the rotating and stationary manometers served to reduce capillarity inconsistencies.

The outlet total head tube is subjected to a periodic flow of varying direction and energy content. Since the yaw insensitivity of a kiel probe is $\pm 40^{\circ}$ (Ref. 13) an "average" total head is measured. Whether or not this reading truly represents the discharge head is discussed in a later section.

For determination of flow patterns within the impeller passages, small, simple total head probes were installed in the impeller passages pointing into the relative flow. The tubes were formed from 1/16 in. brass tubing about three inches long with a 1/4 in. leg. The opening was bored out with a drill point until quite sharp and conical. Such probes are fairly insensitive to yaw (about $\pm 20^{\circ}$) thus permitting relative total head readings to be made with a minimum of angular adjustment.

Experimental Work and Procedure

In experimental work on turbomachines essentially two types of information are sought. The first is the behavior of over-all performance; for example, the measurement of torque, speed, head developed, and flow rate. The second is a knowledge of the details of the flow process. The measurement of pressure distributions, internal velocity

profiles, losses, etc., are in this latter category. In this present work, data of both kinds are taken in order to check the suppositions of the theory.

The following experimental data were obtained in the three test impellers:

i. The head vs. flow rate relation was determined from zero flow to near choke off (i.e., zero head).

ii. Pressure distributions over a range of flow rates from shockless to approximately one-half of that.

iii. Internal head and static pressure surveys were made at a passage inlet and at a passage outlet section for various flow rates on the 6-vaned impeller. The design of the impeller drive mechanism did not allow torque to be measured for these tests.

The tests outlined above were run at rotative speeds from 150 to 200 rpm. The inlet and discharge total pressures were measured with the probes described in the preceeding section. The kiel probe was mounted 1/8 in. away from the impeller outside diameter to measure the discharge total pressure, and during use it was found that the dependence of the kiel probe reading on the angular setting was slight. These tests were run at about 200 rpm. Manometer error due to capillarity differences was a maximum of 0.003 ft. water. At flow rates for which the discharge pressure was steady ($\phi < 0.1$), the error in head measurement was about three-quarters of a percent or less of the maximum head reading. The developed head was measured at three stations over the breadth of the discharge passage; namely, 1/4, 1/2, and 3/4 in. over the bottom shroud. The head measurements were made with increasing values of flow rate; however, checks with the procedure reversed failed

to show any difference. The results of the head vs. flow rate tests are shown in Figs. 12, 13, and 14, together with the computed characteristics.

Experimental pressure distributions at the center section of the vanes were obtained for the three test impellers using the rotating manometer and the technique described in the foregoing paragraphs. The flow-rate coefficient was varied from φ_e (shockless entry) to about $\varphi_e/2$ in each case. During the tests, care was taken that the manometer ran true and that air bubbles were not trapped in the tubing connecting the piezometer taps to the manometer. The manometer tubes were relatively small (5 mm.) and apparently they were not all of the exact same size since a few of them showed capillarity differences on the order of 0.02 ft. maximum. The results of these tests and the computations are presented in Figs. 8, 9, and 10.

One of the principal assumptions of the theory is that the flow is the same at all stations across the breadth of the impeller. In any real impeller the flow must be turned from an axial to a radial direction during or before it enters the vane system. If in such a turn the wall curvatures are too great, the viscous properties of the fluid may result in the detachment of the main flow from the boundary and/or the growth of a region of retarded velocity. Among other things, the immediate result is that the flow scheme is different from that supposed by the theory. To investigate whether or not these phenomena actually occur, internal flow surveys were made on the N = 6 impeller at two radii. The first was taken a short distance behind the vane inlet edges ($r/r_2 = 0.646$) to determine the effect of the large curvature of the inlet shroud on the flow and to see if the vane leading edges separated. The second survey was conducted near the vane tips ($r/r_2 = 0.938$) in order to ascertain the

magnitude of the losses developed within the passage.

In these surveys 1/16 in. impact tubes were installed in the impeller passages pointing into the flow at an angle equal to the vane angle. Piezometer taps 0.030 in. in diameter were drilled on the top and bottom shrouds to measure static pressure. Although the static taps were all put in one passage, it was believed that to do so with the total head probes would result in undue blocking of the passage. Accordingly, eleven such probes were distributed in the six identical passages of the impeller. Total head measurements were made at six different elevations over the bottom shroud for the inlet survey and five for the exit. Results of these surveys are shown in Figs. 15 to 18, but their discussion is deferred to a later section.

Treatment of Experimental Data

a). Computation of Efficiency. The lack of measured torques precludes the exact computation of efficiency. However, the measured pressure distributions give the normal forces exerted on the fluid, and from this information an "input" head or work coefficient ψ' can be derived. It is this quantity rather than the developed head ψ_d which should most closely agree with the theory. This coefficient is computed from the equation

$$\psi' = \frac{N}{4\pi\phi}\int_{\frac{r_1}{r_2}}^{1} \Delta C_p\left(\frac{r}{r_2}\right) d\left(\frac{r}{r_2}\right) \qquad (25)$$

in which ΔC_p is the measured pressure loading coefficient. The work coefficient ψ' and the developed head coefficient ψ_d differ by the fluid energy losses, and a "hydraulic" efficiency may then be written as

$$\eta = \frac{\psi_d}{\psi'} \qquad (26)$$

Equation (26) may be regarded as an approximate measure of the efficiency of the impeller since ψ' represents the energy input to the flow (apart from tangential friction forces) and ψ_d the output energy. Due to variation of the relative total head across the passage, additional mixing losses are encountered after the impeller. Such losses are not included in this computation of efficiency. For N = 6 this efficiency is about 95 percent and it has a substantially flat peak in the range of flow rates φ = 0.12 to 0.20 (Fig. 12). Similar results are observed on the 4-bladed impeller; however, the peak efficiency for N = 2 is much lower, being about 80 percent. The measured head varied somewhat from top to bottom shroud. For efficiency determination the head at the passage center was used; although at flow rates for best efficiency the head was practically constant across the passage width.

b). Computation of "Relative Head Loss". The term "total head loss" requires some explanation when used in connection with the relative flow. The Bernoulli equation for rotating coordinates, i.e.,

$$p + \tfrac{1}{2}\rho\left[W^2 - r\omega^2\right] = \text{const.}$$

is rigorously true if the absolute flow or the flow observed in a stationary coordinate system is incompressible, irrotational and inviscid. If the relative flow total pressures $p + \frac{1}{2}\rho W^2$ are then compared at the same radius on a rotating manometer, they will read the same since the centrifugal effects are cancelled out in the tubing connecting the manometer to the total head measuring device. Thus, if the flow is a potential flow, the difference between, say, the inlet total pressure and any other total pressure as read on a rotating manometer is zero. A departure from zero is designated as a "loss". This loss should not necessarily be interpreted as a reduction in the discharge total pressure, since the static

pressure and the absolute velocity pressure $\frac{1}{2}\rho C^2$ constitute the total discharge pressure. In order to compute the total pressure rise, the relative loss and the direction as well as the magnitude of the relative velocity must be known. However, as a first approximation, these losses can be considered as static pressure reductions.

Contour plots of the relative loss coefficient ζ_r for the 6-vaned impeller are shown in Figs. 15 to 18. The loss coefficient is defined as

$$\zeta = \frac{P_T - P_t}{\frac{1}{2}\rho U_2^2}$$

where P_T is the inlet total pressure and P_t is any other relative total pressure. These plots show the regions most affected by viscosity, and give a good qualitative idea of the flow. By using these loss contours and the relative velocities (not shown) calculated from the flow surveys, a weighted loss coefficient may be obtained, i.e.,

$$\overline{\zeta}_r = \frac{\int \zeta_r W dA}{\int W dA} \tag{27}$$

To be completely correct, each of these integrals should contain a factor $\sin \beta_f$ where β_f is the angle between the relative velocity and a normal to the radius at that point. Experimentally it is quite difficult to measure this angle. For the purposes of computation it is assumed to be constant and as a consequence of the value of $\overline{\zeta}_r$ may be low.

With the coefficient $\overline{\zeta}_r$ defined above, an order of magnitude check of the efficiency as computed by Eq. (26) may be made. If skin friction forces are not too important, then the energy input to the flow is approximately given by $\psi_d + \overline{\zeta}_r/2$, hence

$$\eta = \frac{\psi_d}{\psi_d + \frac{\zeta_r}{2}}$$

Evaluation of $\overline{\zeta}_r$ for $\varphi = 0.238$ gave 0.07 for the exit survey. The efficiency computed by this relation is 87 percent, whereas Eq. (26) gives 84. At $\varphi = 0.178$ the two methods agree to within 2 percent. It is not desired to belabor this point unnecessarily but considering the experimental accuracy this agreement is taken to mean that the "hydraulic" efficiency as computed here is probably accurate to within 2 percent and that the method of measuring the developed total head is accurate to the same order.

IV. COMPARISON OF THEORY AND EXPERIMENT

From comparison of measured and calculated distribution of pressures afforded by Figs. 8, 9, and 10, it is immediately evident that the theoretical results do not satisfactorily agree with the actual measurements, particularly for flow rates near shockless entry. The agreement is best for the 4- and 6-vaned impellers at flow rates of about $\varphi = 0.14$ to 0.18. The measured head coefficients (Figs. 12 - 14) also deviate considerably from the theoretically predicted ones near shockless entry but at flow rates substantially less near $\varphi = 0.18$ the disparity is ten percent or less. The values of the work coefficient obtained from the measured pressure distributions agree fairly well with the computed values near $\varphi = 0.18$ for all impellers, although its slope is steeper than the predicted head vs. flow rate line.

The fact that the discrepancy between the observed and computed quantities becomes greater as shockless entry is approached is rather surprising. It is usually expected that agreement between potential flow calculations and experiment will be best when sharp velocity peaks at leading edges are avoided. For flow in pump impellers this condition

is satisfied at shockless entry. The experimental fact that the pressure distributions and work coefficient are in poor agreement here strongly suggests that phenomena not necessarily connected with the vanes alone have become important enough for these flow rates to change the flow.

The inlet surveys taken on the N = 6 impeller (Figs. 15 - 18) show that for a flow rate of $\varphi = \varphi_e = 0.238$ the flow is scarcely potential. On the leading face of the vane (pressure side) and on the bottom shroud, substantial regions of high loss occur. These losses are diffused throughout the passage and a further increase in boundary layer occurs as is evidenced in the exit survey. Part of the "diffusion" of the high loss areas is, no doubt, due to secondary flows in the passage which originate from the nonuniformities in relative total head. Static pressure measurements, made at the inlet on the top and bottom shrouds, show differences on the order of 15 percent at mid-passage supply further evidence of the nonuniformities of the flow pattern at this operating point. Such differences were not observed at lower flow rates.

It is fairly clear now how the discrepancy between theory and experiment arises at this flow rate. The fact that the experimentally determined value of shockless entry still agreed fairly well with the predicted one is surprising. Possibly it might be conjectured that the "effective" profile of the blade was sufficiently changed by wakes present on the blades to account for this coincidence.

The condition of the inlet flow as seen in Fig. 15 is indicative of the profound effect the inlet and shroud design can have on the entire impeller performance. The abrupt turn and large curvature of the approach section immediately before the bottom inlet shroud (Fig. 7) gives rise to a relatively thick boundary layer (if not local detachment) along the bottom

shroud and a nonuniform velocity across the passage height. At the vane leading edge the approaching fluid is accelerated by the small radius of curvature of the bottom shroud, and, although these velocities were not measured, it is clear that high local velocities must occur there. The immediate result is that the angle of attack is higher near the bottom shroud than at the top and consequently the flow on the bottom separates prematurely. The over-all shape of the loss-contour curves indicates that such an effect may occur. At low rates of flow (much less than shockless) it would be expected, because of the higher velocity on the inlet bottom shroud, that the reverse situation should take place, i.e., separation on the top shroud should now be more severe. The loss contours of Fig. 18 support this argument; however, more information is required to discuss the details of the structure of the incoming flow.

The operating point designated as "shockless entry" is usually taken to be the "design" point as well since it is not desired that regions of large underpressure or high local velocity exist for reasons of cavitation or gas evolution. With the present apparatus the inlet turn is of great importance to the over-all behavior at flow rates for which shockless entry occurs on these impellers. Consequently, it would seem appropriate to make comparisons where inlet conditions are the most favorable, even though large underpressures may exist. Inspection of the loss distributions given in Figs. 15 - 18 shows that at a flow-rate coefficient of $\varphi = 0.178$ the inlet portions of the vanes are relatively free of wakes. Typically, however, a fairly large boundary layer still remains on the bottom shroud. The agreement of both the developed head (Fig. 12) and measured distributions of pressure with the computations is seen to be relatively good at this flow rate. Reasonably favorable

entrance flows are found to occur in the range of about $\varphi = 0.14$ to $\varphi = 0.20$ and in this region not only are the work coefficients nearly equal to the predicted head, but the pressure distributions are fairly close.

Thus far, all comparisons have been made at flow rate coefficients based on the total discharge. Actually the presence of boundary layers and the thickness of the vane result in a velocity increase of the effective part of the stream. This effect may be roughly taken into account by comparing the experimental results to computations evaluated at flow rates higher by an appropriate amount.

Such a comparison can only be realistic when the flow is not greatly disturbed by zones of separation on the vanes, that is to say, when the entrance conditions are best. At a flow rate coefficient of $\varphi = 0.178$ an approximate measure of the boundary layer influence is provided by a plot of the relative velocity across the passage height, mid-way between the vanes at an entrance and an exit section (Fig. 19). The velocity ratio of the main flow to the average is 1.06 at the inlet. Vane thickness accounts for seven percent of the peripheral area at the inlet and four at the exit. A reasonable estimate of the effective flow rate would be then around ten to twelve percent more than the average flow rate. Comparisons of measured and computed distributions of pressure on this basis are presented for $\varphi = 0.178$, $N = 6$ (Fig. 20) and for $\varphi = 0.18$, $N = 4$ (Fig. 21). It is seen that the agreement is better than for the unadjusted theory, and that the corrections made are in the right direction. At a corrected value of $\varphi = 0.178$ the predicted head for $N = 6$ becomes close to the measured work coefficient, but the pressure distribution loops are still somewhat lower than called for by the theory. Part of

this discrepance is due to inlet losses which are still present.

The actual state of affairs is certainly more complicated than the simple adjustment of flow rate might indicate. Not only is the main flow speeded up, but a boundary layer develops along the vane faces which results, essentially, in a blade profile different from that originally assumed. This fact is supported by the thick layer of high loss fluid on the vane trailing side seen in the exit relative flow surveys and it is suggested by the general progressive downward shift of the experimental pressures from the calculated ones. The loss contours of Figs. 15 - 17 all show substantial boundary layer developments on the trailing faces of the vanes. Roughly speaking, this effect is to reduce the vane angle which in turn results in a steeper head vs. flow rate line. In the region of best efficiency this effect would account for the increased slope of the work coefficient line.

Comparisons made thus far have been based on average and effective flow rates. It is also possible to evaluate the theory at the same head or circulation as that experimentally found. However, if the circulation is changed from that required by the theory, then the Kutta condition is no longer satisfied and infinite velocities occur at the vane tips. For that reason such computations are not presented.

The general behavior of the two-bladed impeller followed that of the 4- and 6-vaned ones. The discrepancy in pressure distributions is, in general, somewhat more than for the others; however, as before, the theoretical head provides a good estimate of the work coefficient. The efficiency, though, is lower than the $N = 4$ and $N = 6$ runners and has a maximum value of only 80 percent. As in the other cases, the experimentally determined value of shockless flow rate is nearly equal to the

predicted value. The high value of the developed head near shut-off is interesting since, in order to achieve heads substantially higher than the theoretical value, a large part of the flow must rotate like a solid body.

Effect of Number of Vanes

For a given vane angle and radius ratio the effect of number of vanes for a pump is similar to the effect of solidity in a two-dimensional cascade. For commonly employed impeller parameters the head developed is nearly proportional to the number of vanes if there are only a few present, i.e., two or three. If the number becomes appreciable, say six, then the effect of mutual interference becomes important and the head developed rapidly approaches the maximum given by the infinite vane theory. Low values of N have low values of the coefficients ψ_0 and C_v resulting in lower and flatter head vs. flow rate lines as seen progressively in Figs. 12 to 14. However, for low numbers of blades the pressure loading per vane is high. Since the pressure cannot exceed that of a forced vortex, the practical result is that blade static pressures for N = 2, 3, 4, etc., are much lower than for N = 6 or 8. This trend is readily seen in the plots of computed pressure distributions, Figs. 3 - 5.

A result of a large number of vanes is the suppression of large scale separation or flow detachment from the vane leading edges. This effect is observed in Figs. 8a, 9a, and 10a wherein the progressive departure with decreasing N of the measured and calculated pressures on the low pressure (trailing) side is seen.

The low heads and high loadings of impellers with only two or three vanes place them at a great disadvantage. For these reasons their use is limited to very special applications.

Situations of the sort found in this work are not uncommon in the

application of potential theory to problems in the flow of real fluids. Pinkerton (Ref. 14) in a study of measured and calculated pressure distributions on the N. A. C. A. 4412 Airfoil observed discrepancies in lift coefficient of 20 percent when computed by usual methods. At moderate angles of attack, measured and experimental distributions of pressure disagreed in much the same way as they were found to in this work. However, he was able to "adjust" the airfoil profile to account for the progressive development of the boundary layer in such a way as to obtain excellent agreement of the computed and measured distributions.

The flow within the passages of centrifugal pump impellers is much more complex than that over an airfoil. The regions of fluid affected by viscosity are larger and secondary flows caused by the nonuniformities in relative total head occur. The low aspect ratio of the passage also enable viscous effects to become more important than for the flow over airfoils. In this work it would have been possible to change the vane profile to account for some of the boundary layer effects as Pinkerton has done for airfoils; however, this process for a circular array of vanes is much more laborious than for a single profile. Moreover, for the cases studied, the inlet conditions were not ideal. For these reasons computations along such lines were not considered to be worthwhile at present.

Application to Design

In view of the limited data available on vane angles and radius ratios, a discussion of design application can be regarded only as tentative at least for the present. However, a few remarks on the usefulness of these results are in order.

It has been found that the theory gives a good estimation of the work coefficient when the flow in the inlet portion of the impeller is good. For the cases studied, the range of flow rates for reasonable inlet conditions

was about $\phi = 0.16$ to 0.20. In other terminology this corresponds to a local geometrical angle of attack of -1° to $+4^{\circ}$ based on the average relative inlet velocity and the inlet vane angle. Furthermore, in this range the measured and theoretical pressure distributions agree fairly well if the flow rate is changed to account for vane thickness and an estimate of the shroud boundary layer. For moderate numbers of vanes (at least four or greater) the "hydraulic" efficiency is relatively high, being about 94 percent. There is no reason to use any less than four vanes except for special applications, e.g., slurry pumps. Hydraulicly, it would seem preferable to use six vanes if not more since the overall vane load is reduced with increasing numbers of vanes and severe underpressures are suppressed. It is not likely that any reasonably well-designed inlet shroud will perform more adversely than that used in this work. For that reason it may be supposed that the above statements are conservative and for the present may be used as convenient "rules of thumb" at least for configurations not far different than the ones studied.

V. SUMMARY AND CONCLUSIONS

The measured distributions of pressure and work coefficient were found to agree fairly well with the predicted values when the flow conditions at the inlet of the vane system were best. At flow rates near shockless entry, large deviations were observed which were traced to nonuniformities in the inlet flow arising from the abrupt inlet turn. The fact that the agreement between the potential flow calculations and the experiments is as good as it is for flow rates much less than shockless where pressure discontinuities still occur on the vane inlet edges, is

considered promising. In view of this fact, it seems reasonable to suppose that if a highly uniform inlet flow were supplied to the impeller, then better agreement over a broader range of flow rates would result. The theory as it now stands appears to be useful for design over certain limited rates of flow. Application to wide ranges of operating conditions is still restricted since the inlet turn introduces additional unknown factors.

In view of these remarks, it seems appropriate to outline further work on the following lines:

1. Studies should be made to determine shroud shapes which effectively turn the flow from an axial to a radial direction.

2. Investigations of impellers with other vane angles should be undertaken.

REFERENCES

1. Osborne and Morelli, Head and Flow Observations on a High-Efficiency Free Centrifugal Pump Impeller. Trans. ASME, Vol. 72, No. 7, p. 999 (1950).

2. Prian and Michel, An Analysis of Flow in Rotating Passages of a Large Radial Inlet Centrifugal Compressor at Tip Speed of 700 Feet per Second. N.A.C.A. T.N. 2584.

3. Uchimaru, On Potential Flow of Water Through a Centrifugal Impeller. Journal of the Faculty of Engineering, Tokyo Imperial University, Vol. 19, No. 8 (1931).

4. Busemann, A., Das Förderhöhenverhaltnis radialer Kreiselpumpen mit Logarithmischspiraligen Schaufeln. Ztsch. f. Angew. Math. und Mech. Band 8 Reft 5 (1928).

5. Sörensen, E., Potential Flow Through Centrifugal Pumps and Turbines. N.A.C.A. TM 973.

6. Spannhake, W., Mitteilungen des Instituts fur Stomungsmachinen der Technischen Hochschule Karlsruhe. Heft I. Oldenbourg (1930).

7. Sheets, H. E., The Flow Through Centrifugal Compressors and Pumps. Trans. ASME, Vol. 72, No. 7 (1950).

8. Konig, E., Potentialstromung durch Gitter. Ztsch. f. Angen. Math. and Mech. Bd. 2 (1922).

9. Bateman, H., Partial Differential Equations of Mathematical Physics. p. 243, Dover, (1944).

10. Stepanoff, A. J., Centrifugal and Axial Flow Pumps, p. 39, Wiley (1948).

11. Osborne and Morelli, Measured Performance of Pump Impellers. ASME Paper No. 50-A-90, (1950).

12. Peebles, G. H., A Method for Calculating Airfoil Sections from Specifications on the Pressure Distributions. Journal Aeronautical Sciences, p. 451, Vol. 14 (1947).

13. Report on Kiel Probes. Pratt and Whitney Aircraft. PWA-576.

14. Pinkerton, R. M. Calculated and Measured Pressure Distributions over the Mid-Span Section of the N.A.C.A. 4412 Airfoil. N.A.C.A. Rep. No. 563.

NOTATION

Subscripts

a	-	refers to displacement flows in the w (circle plane)
b	-	refers to the through flow in the w plane
m	-	meridional (radial) component
n	-	normal component
r	-	relative or radial component
t	-	tangential component
u	-	component in the direction of rotation
w	-	refers to quantities in the w plane
Z	-	refers to quantities in the Z plane
1	-	refers to the vane exit tips
2	-	refers to vane entrance tips

Symbols

$Z = x+iy$,	-	complex variable of the physical plane
w	-	complex variable of the mapped plane
$w_o = ae^{i\delta}$,	-	complex constant in the w plane
v	-	vector velocity
V	-	conjugate of vector velocity
U	-	peripheral velocity ($r\omega$)
W	-	relative velocity
C	-	absolute velocity
ω	-	angular speed
N	-	number of vanes
β	-	vane angle
γ	-	complement of the vane angle

Symbols

Γ	-	circulation strength
r	-	radius
q	-	complex constant
C	-	constant for the through flow
ψ	-	head coefficient = head rise/ U_2^2/g
ψ_d	-	measured head coefficient
ψ'	-	work coefficient (input head)
φ	-	flow-rate coefficient = discharge/Exit Area x U_2
p	-	pressure
P_T	-	inlet total pressure
C_P	-	pressure coefficient = $P - P_T / \frac{1}{2} U_2^2$
ζ_r	-	relative loss coefficient

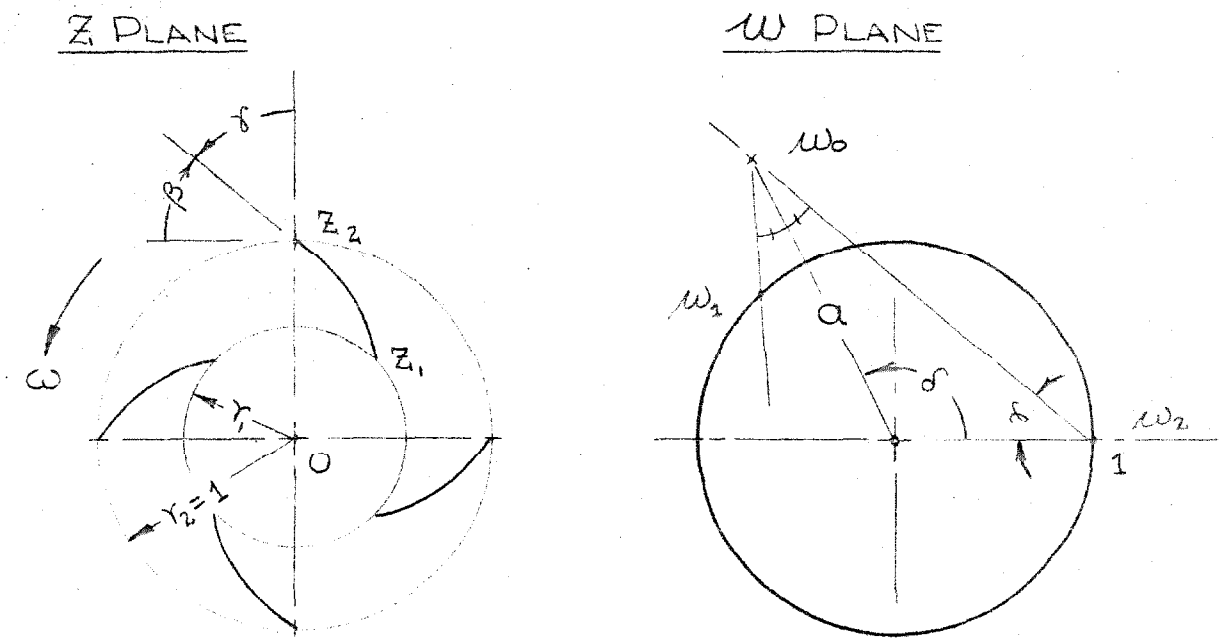

FIG. 1. REPRESENTATION OF BLADE SYSTEM IN THE Z AND w PLANES. POSITIVE DIRECTIONS AS SHOWN.

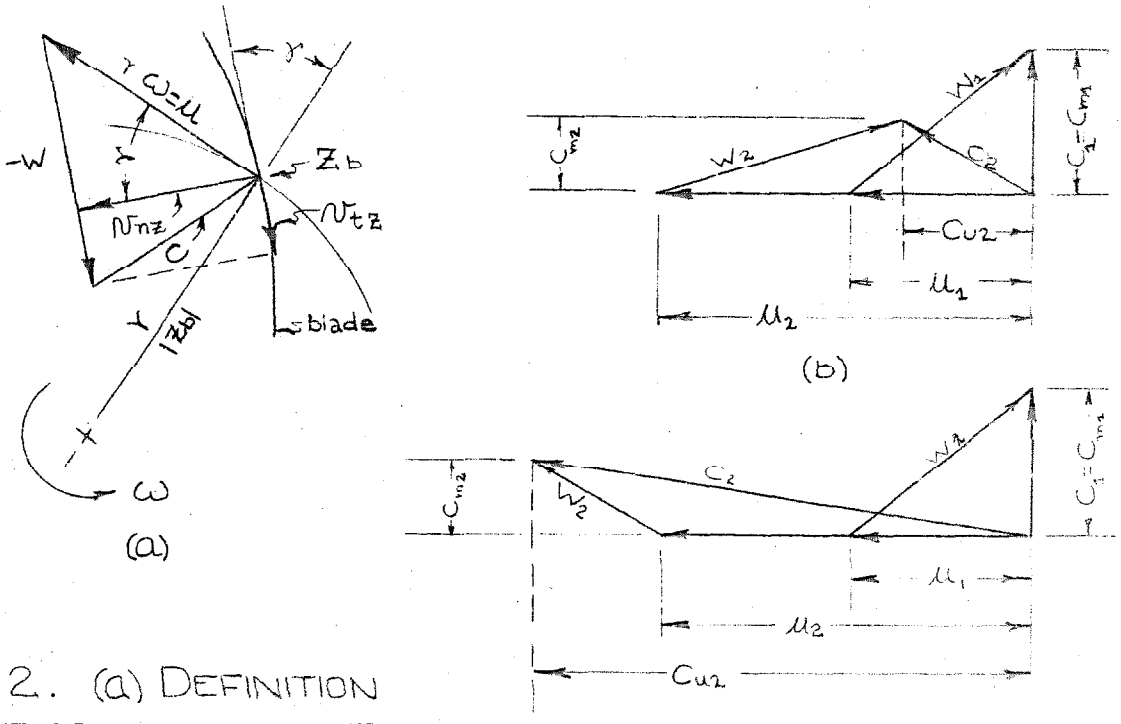

FIG. 2. (a) DEFINITION SKETCH. (b) INLET AND OUTLET VELOCITY TRIANGLES – BACKWARD CURVED VANES, (c) SAME FOR FORWARD CURVED VANES.

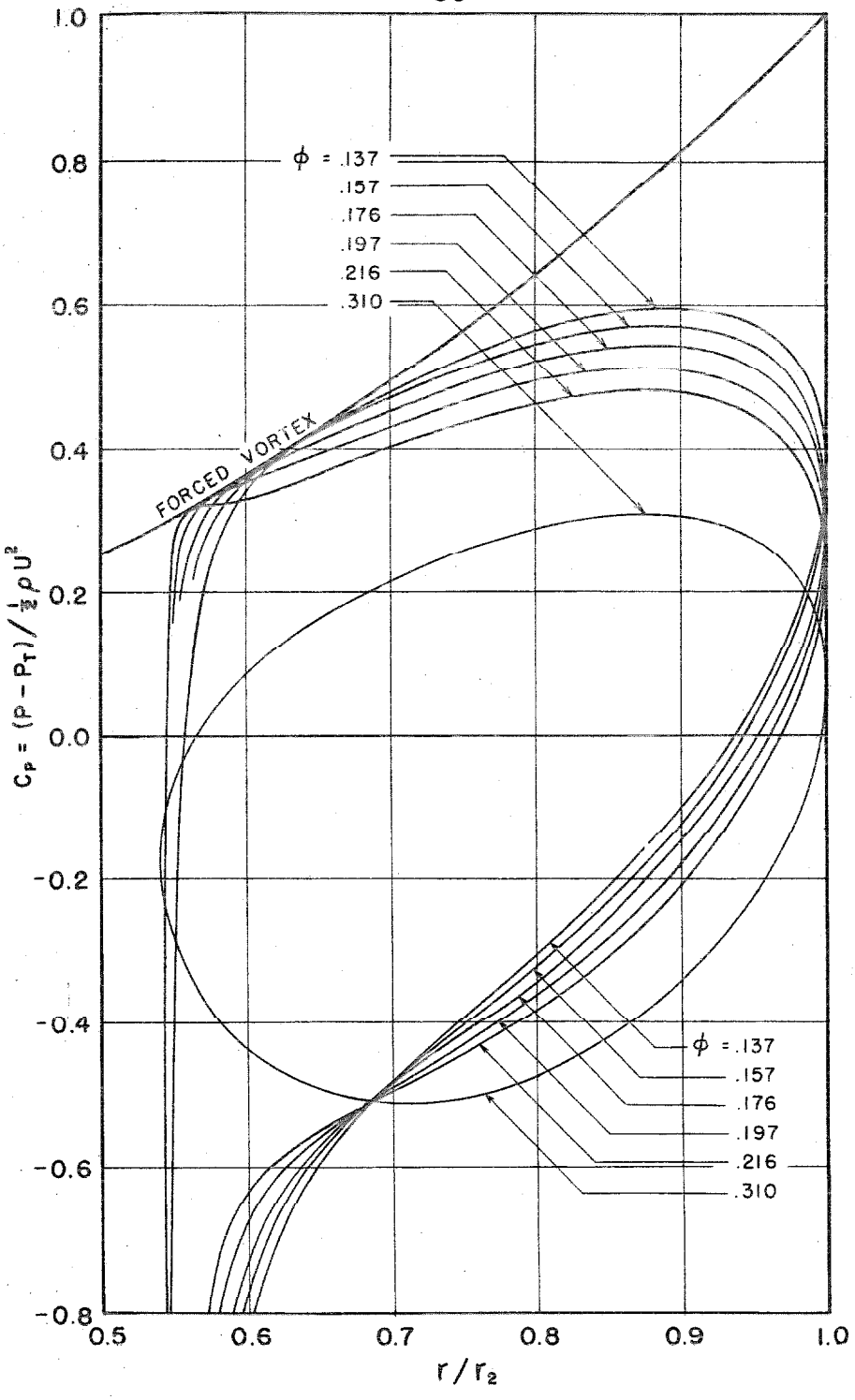

Fig. 3. Theoretical pressure coefficient vs. dimensionless radius at various flow-rate coefficients for an impeller with two, log-spiral, 30° vanes and a radius ratio of 0.54. The forced vortex line represents a limit the theory cannot exceed.

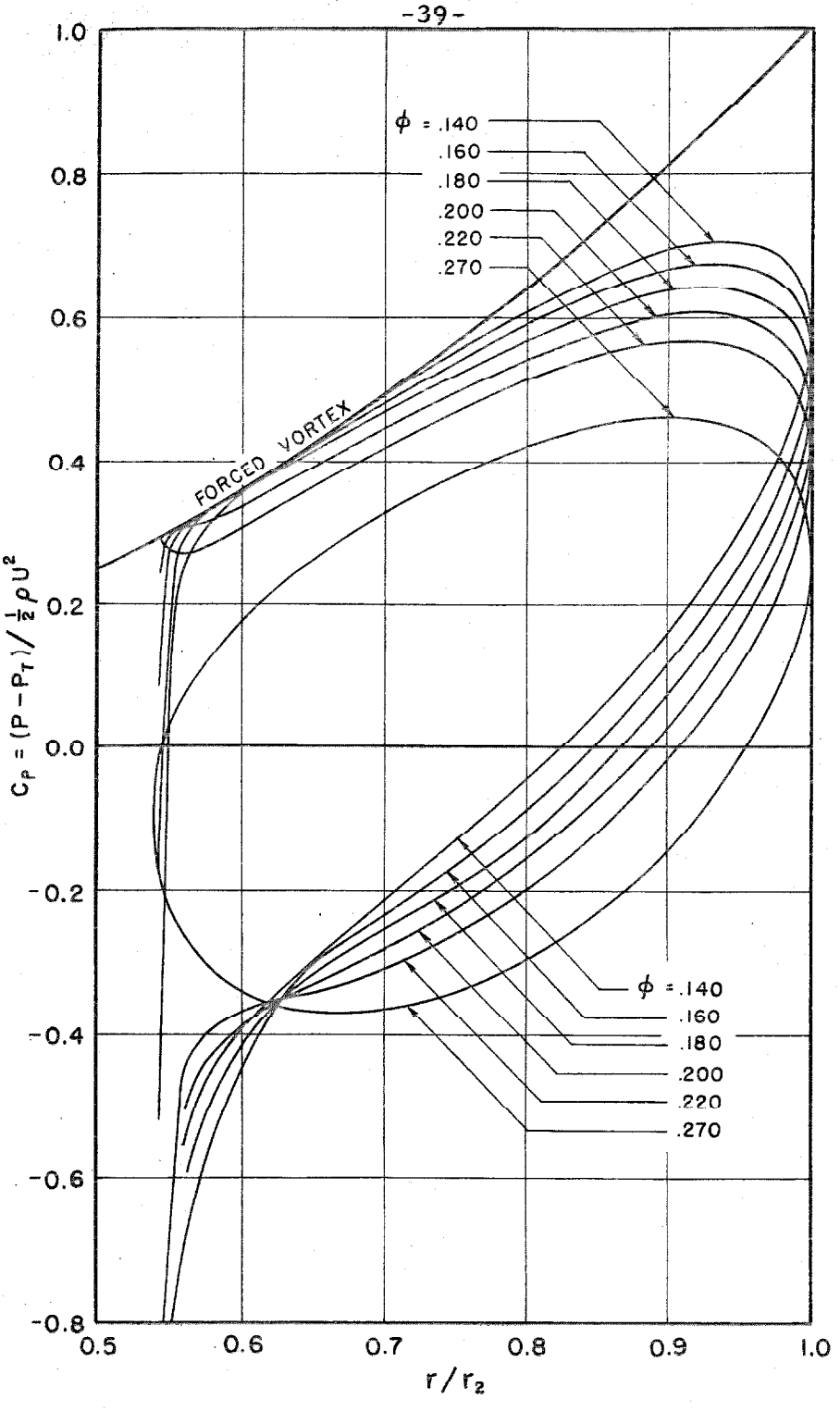

Fig. 4. Theoretical pressure coefficient vs. dimensionless radius at various flow-rate coefficients
N = 4, $r_1/r_2 = 0.54$, $\beta = 30^\circ$.

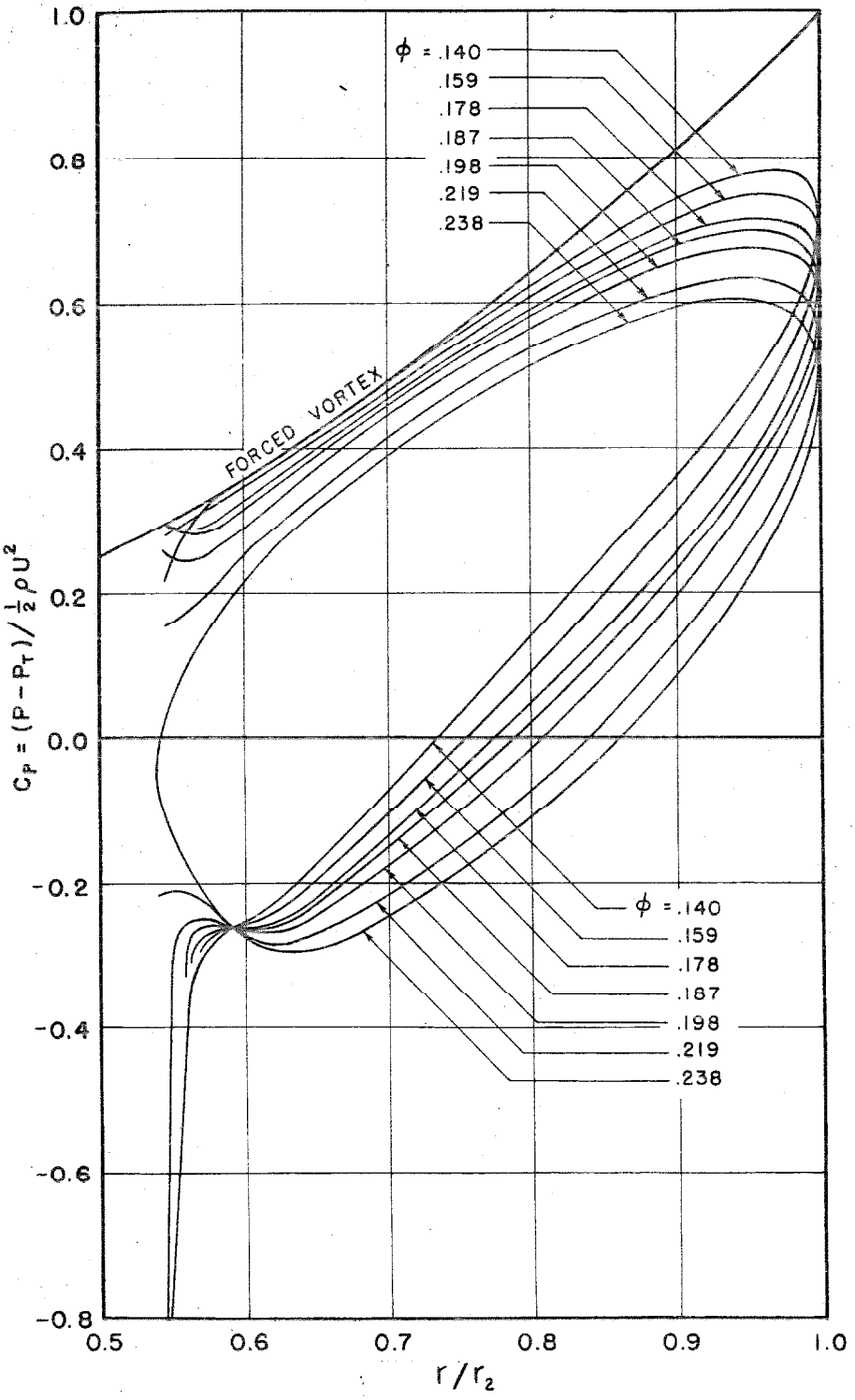

Fig. 5. Theoretical pressure coefficient vs. dimensionless radius at various flow-rate coefficients.
N = 6, r_1/r_2 = 0.54, $\beta = 30^{\circ}$.

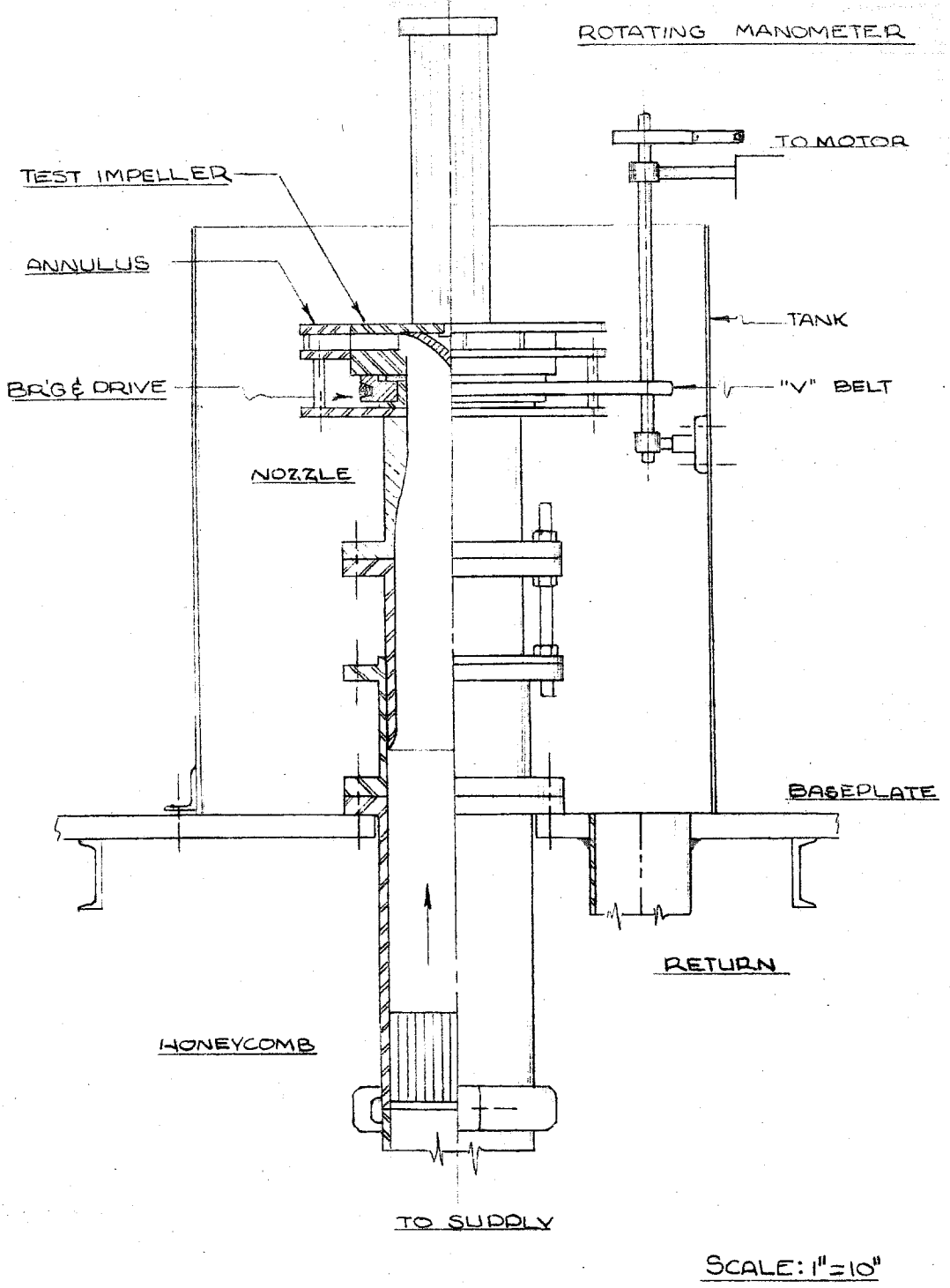

FIG. 6. THE IMPELLER TEST BASIN ASSEMBLY

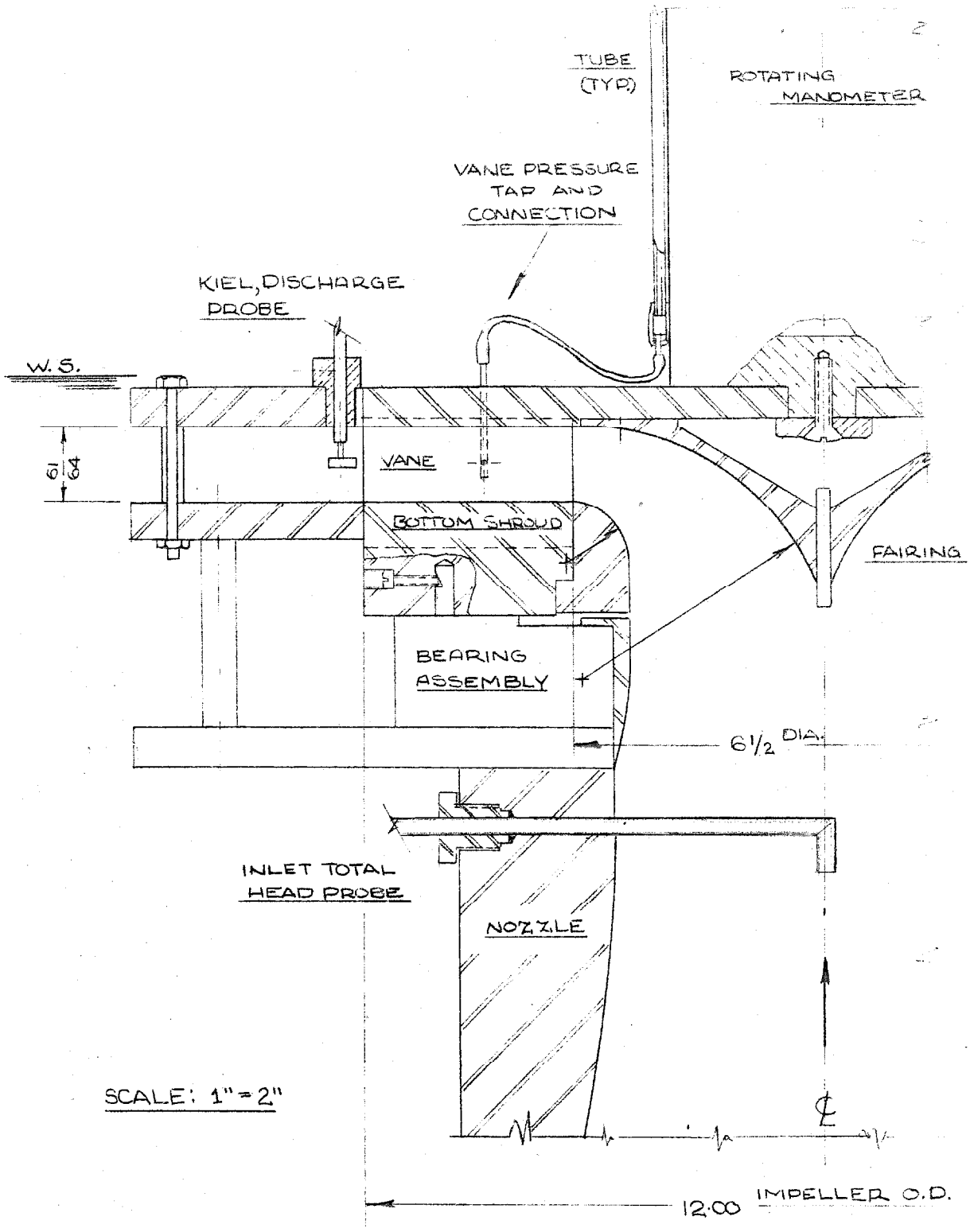

FIG. 7. IMPELLER ASSEMBLY SHOWING INSTRUMENTATION

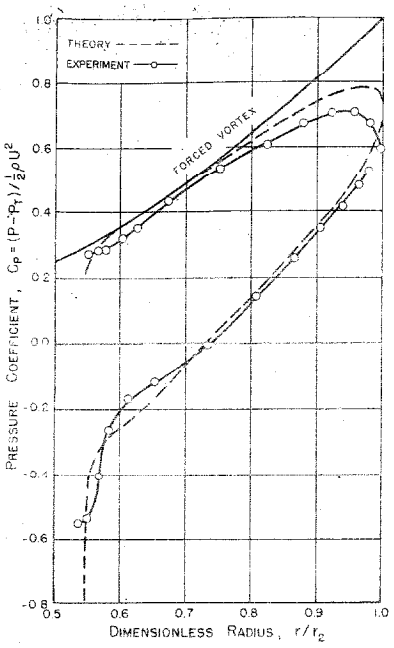

Fig. 8a. $\varphi = 0.140$

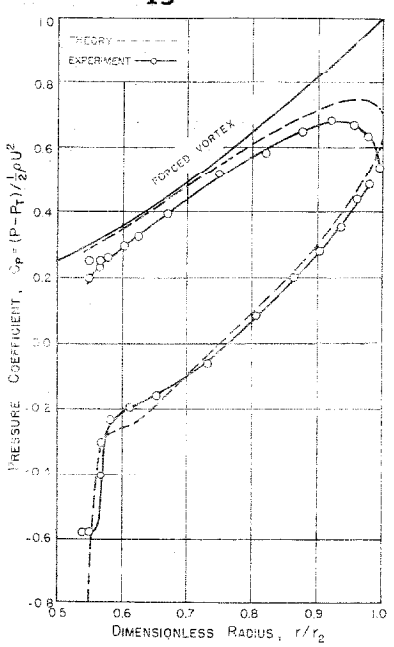

Fig. 8b. $\varphi = 0.159$

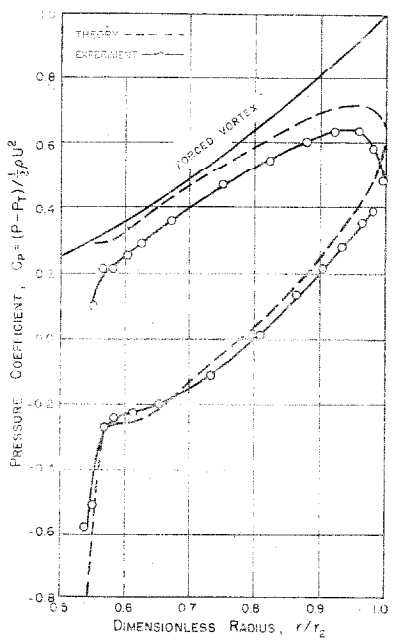

Fig. 8c. $\varphi = 0.178$

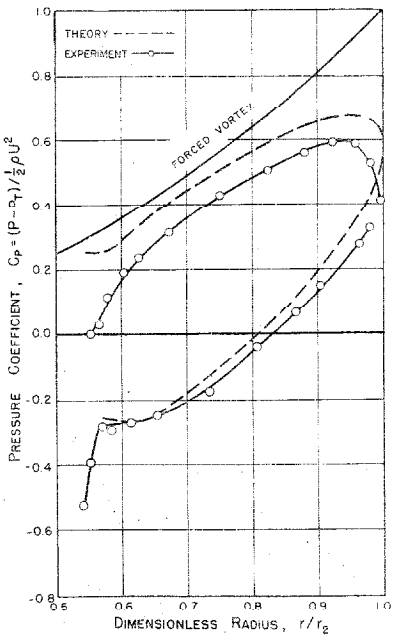

Fig. 8d. $\varphi = 0.198$

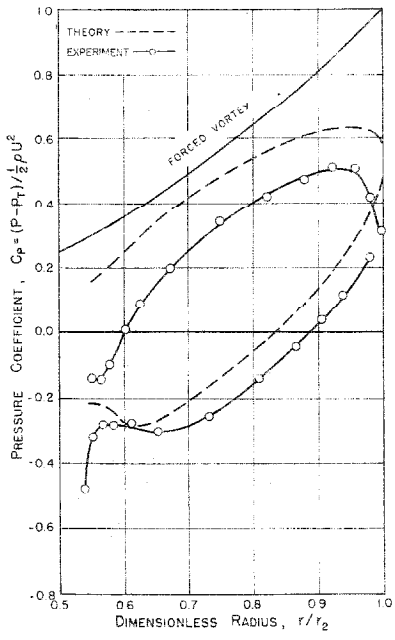

Fig. 8e. $\varphi = 0.219$

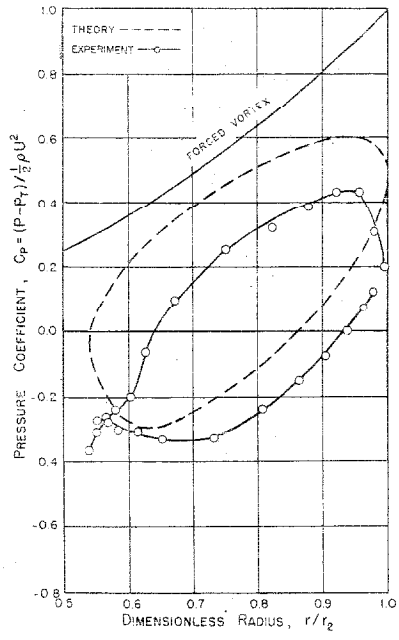

Fig. 8f. $\varphi = 0.238$

Fig. 8. Experimental and theoretical pressure distributions at several values of flow-rate coefficient for an impeller with six, log-spiral 30° vanes and a radius ratio of 0.54.

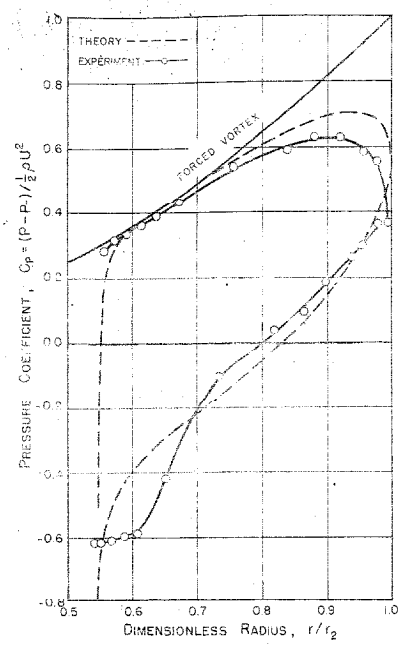

Fig. 9a. φ = 0.140

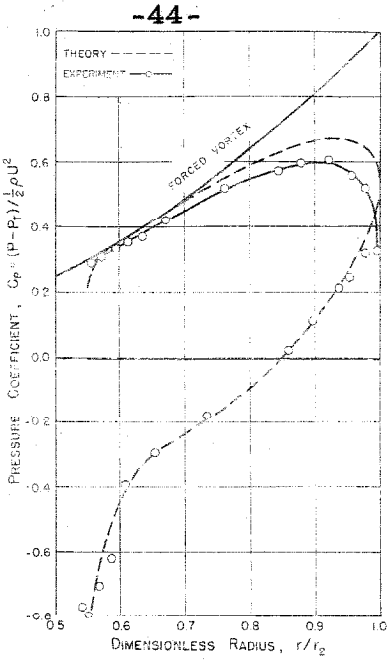

Fig. 9b. φ = 0.160

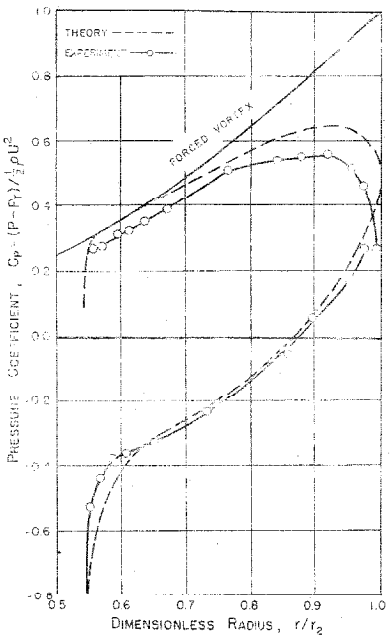

Fig. 9c. φ = 0.180

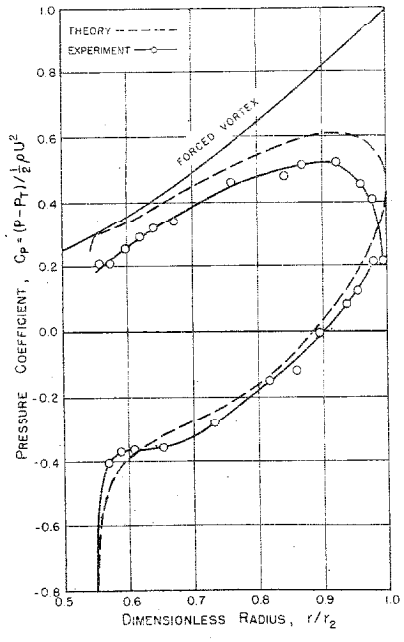

Fig. 9d. φ = 0.200

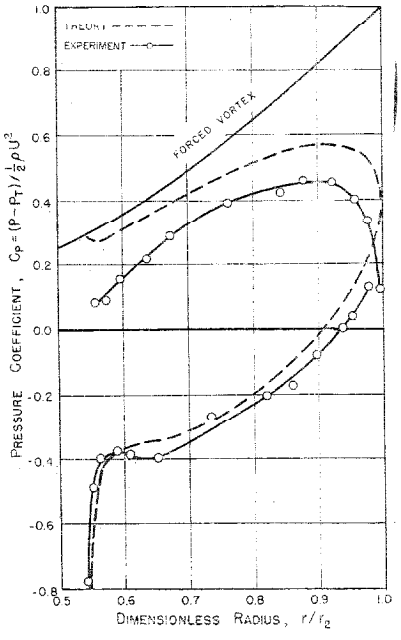

Fig. 9e. φ = 0.220

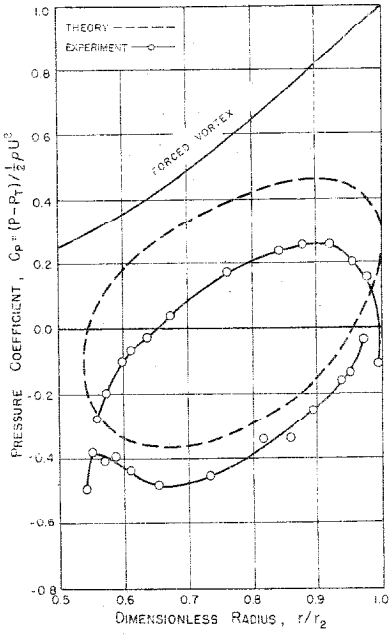

Fig. 9f. φ = 0.270

Fig. 9. Experimental and theoretical pressure distributions at several flow rates for N = 4.

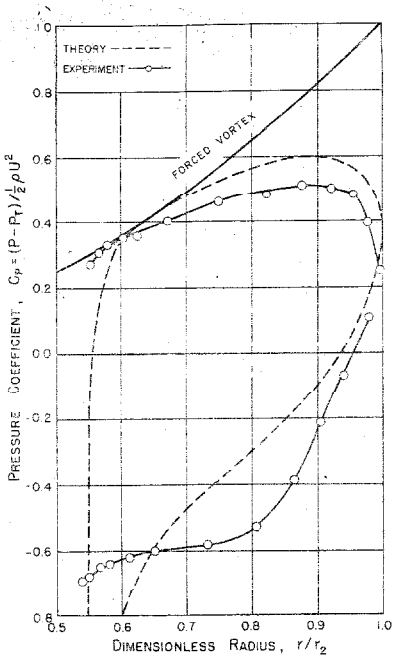

Fig. 10a. φ = 0.137

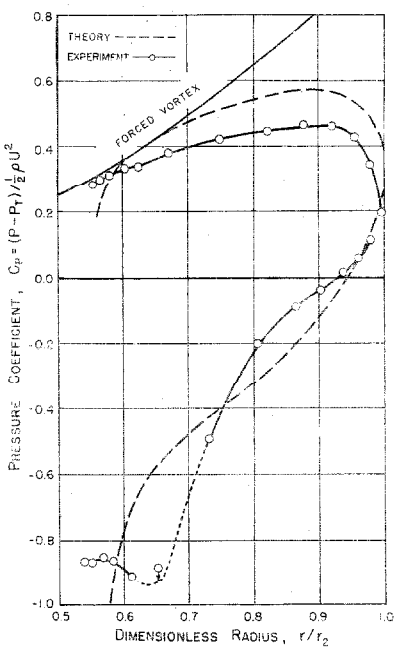

Fig. 10b. φ = 0.157

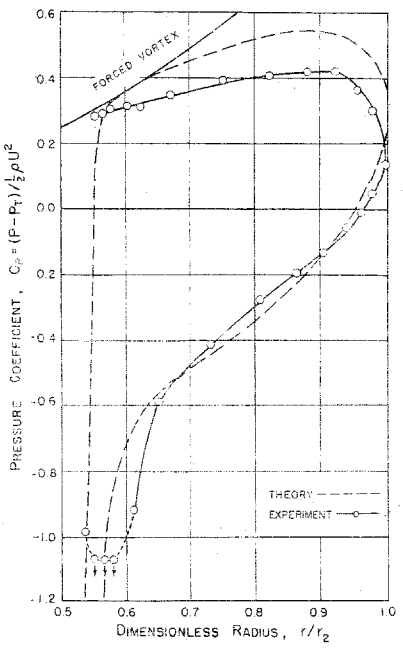

Fig. 10c. φ = 0.176

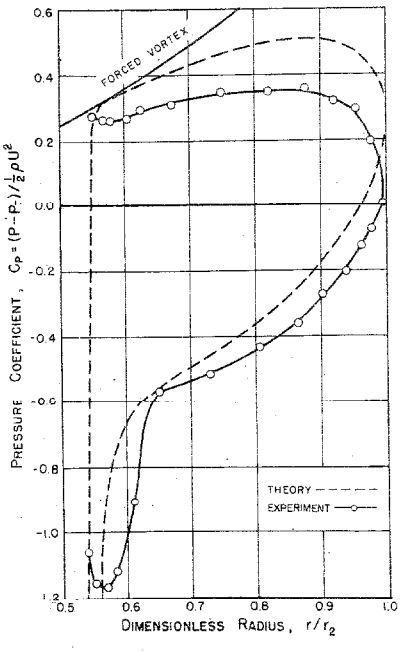

Fig. 10d. φ = 0.197

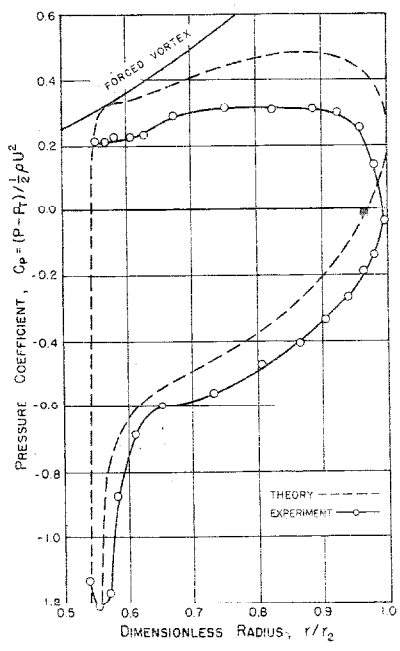

Fig. 10e. φ = 0.216

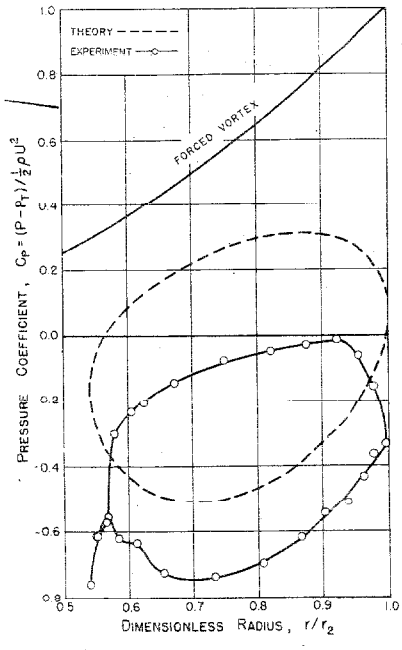

Fig. 10f. φ = 0.310

Fig. 10. Experimental and theoretical pressure distributions at several flow rates for N = 2.

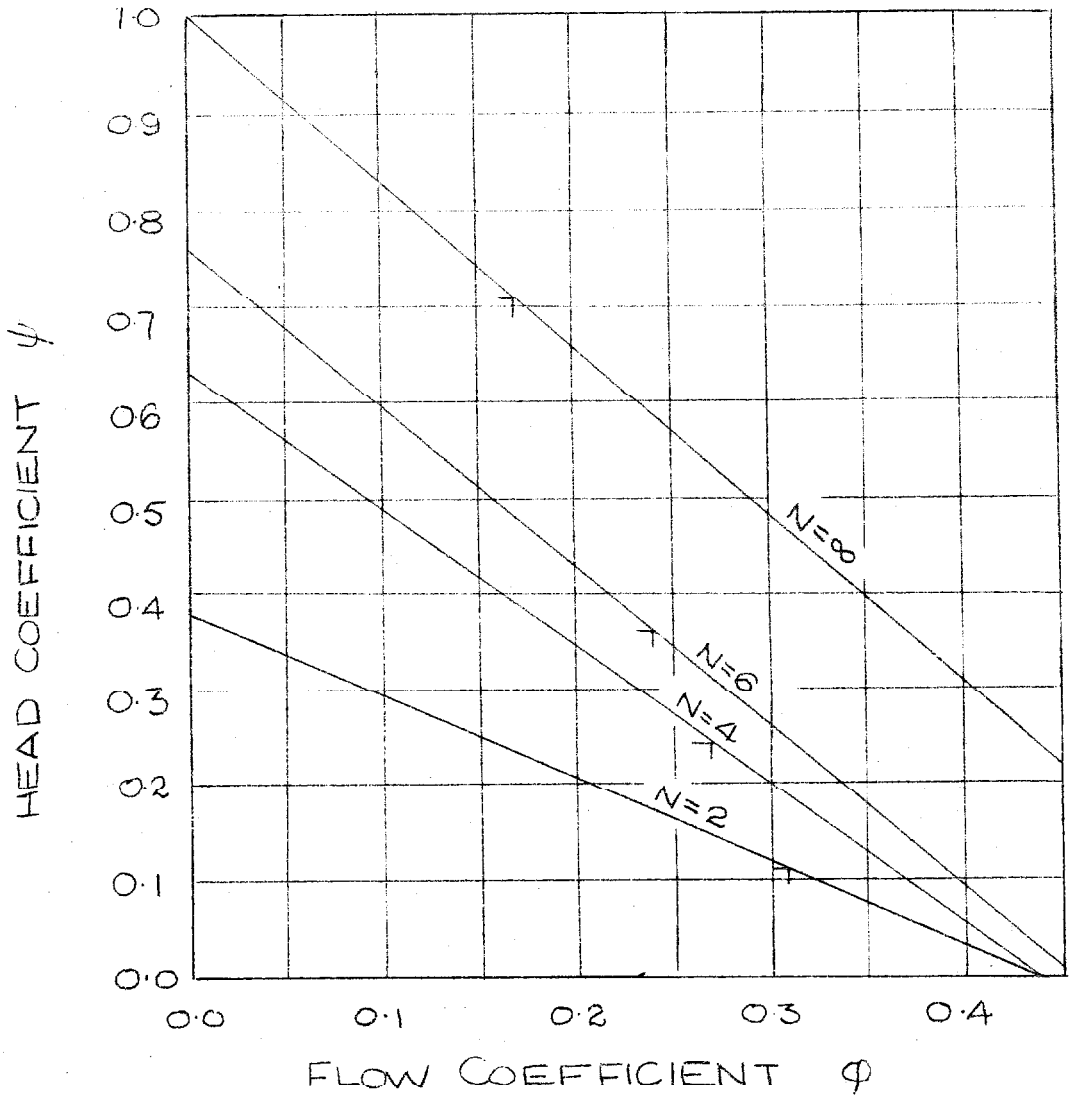

T DENOTES SHOCKLESS ENTRY

FIG. 11. EFFECT OF NUMBER OF VANES ON THE THEORETICAL HEAD VS. FLOW-RATE CHARACTERISTIC.

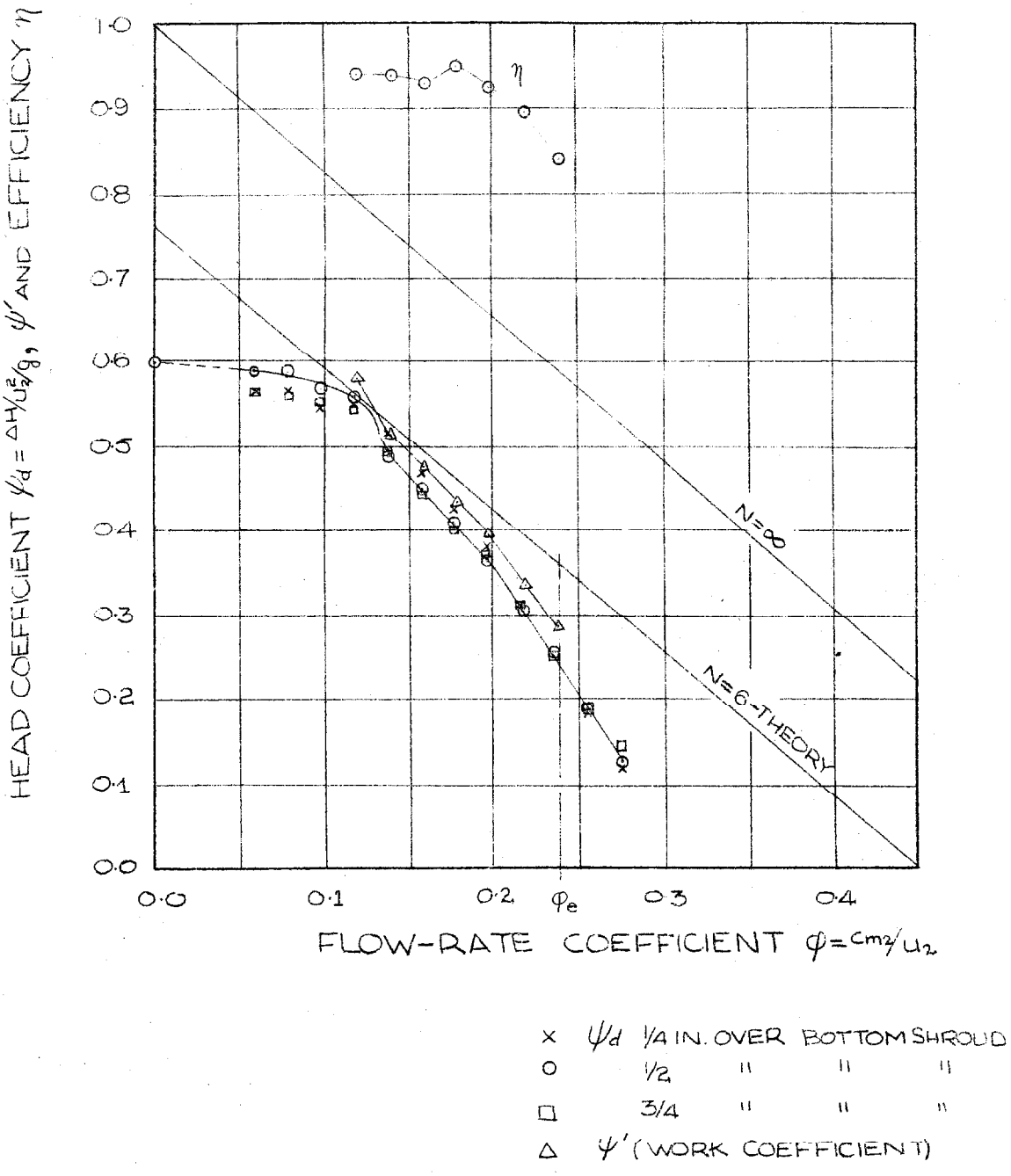

FIG. 12. EXPERIMENTAL AND THEORETICAL HEAD VS. FLOW RATE CHARACTERISTICS. SIX VANES, $\beta = 30°$, $r_1/r_2 = 0.54$.

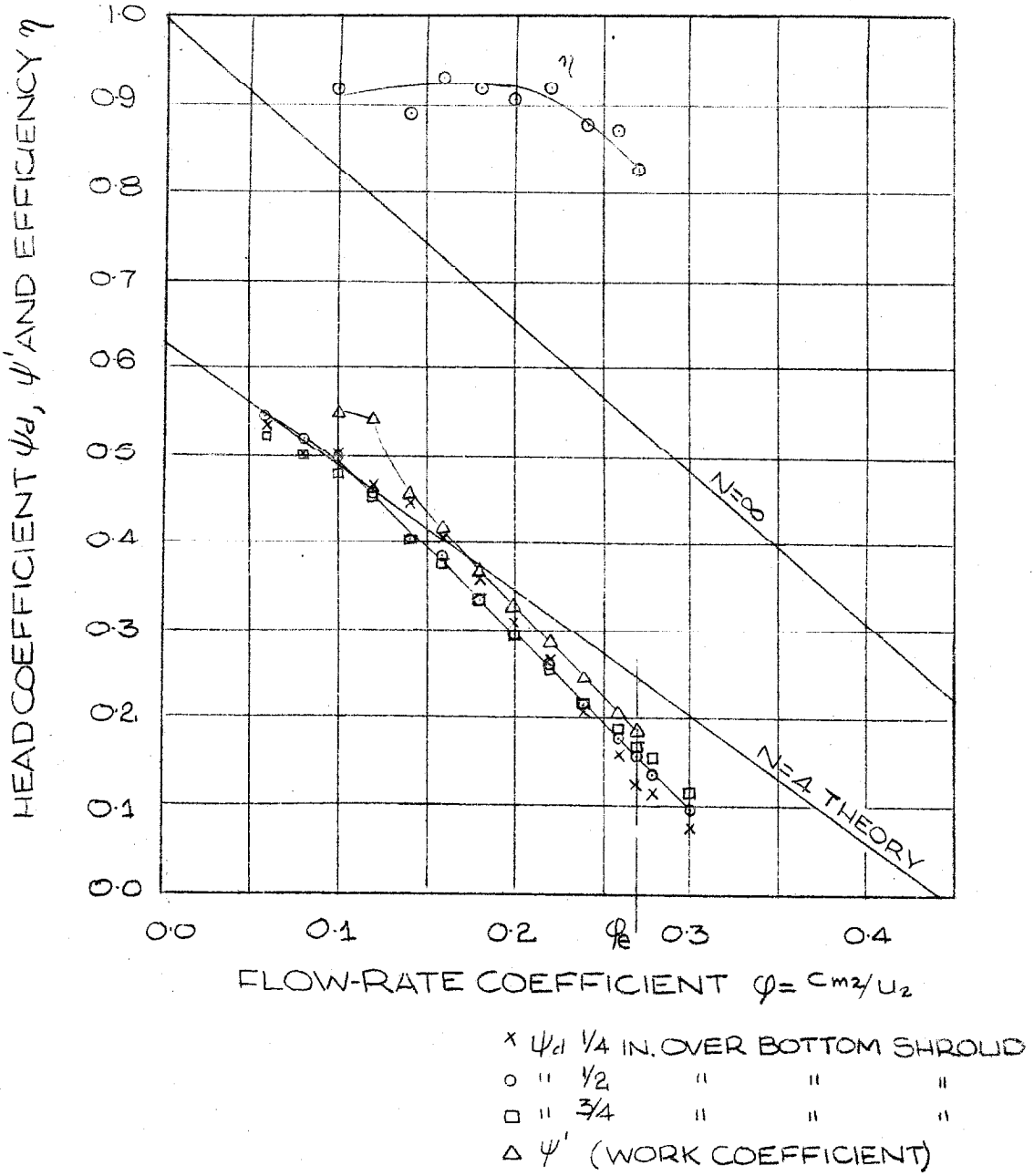

FIG 13. EXPERIMENTAL AND THEORETICAL HEAD VS. FLOW RATE CHARACTERISTICS. FOUR VANES, $\beta = 30°$, $r_1/r_2 = 0.54$.

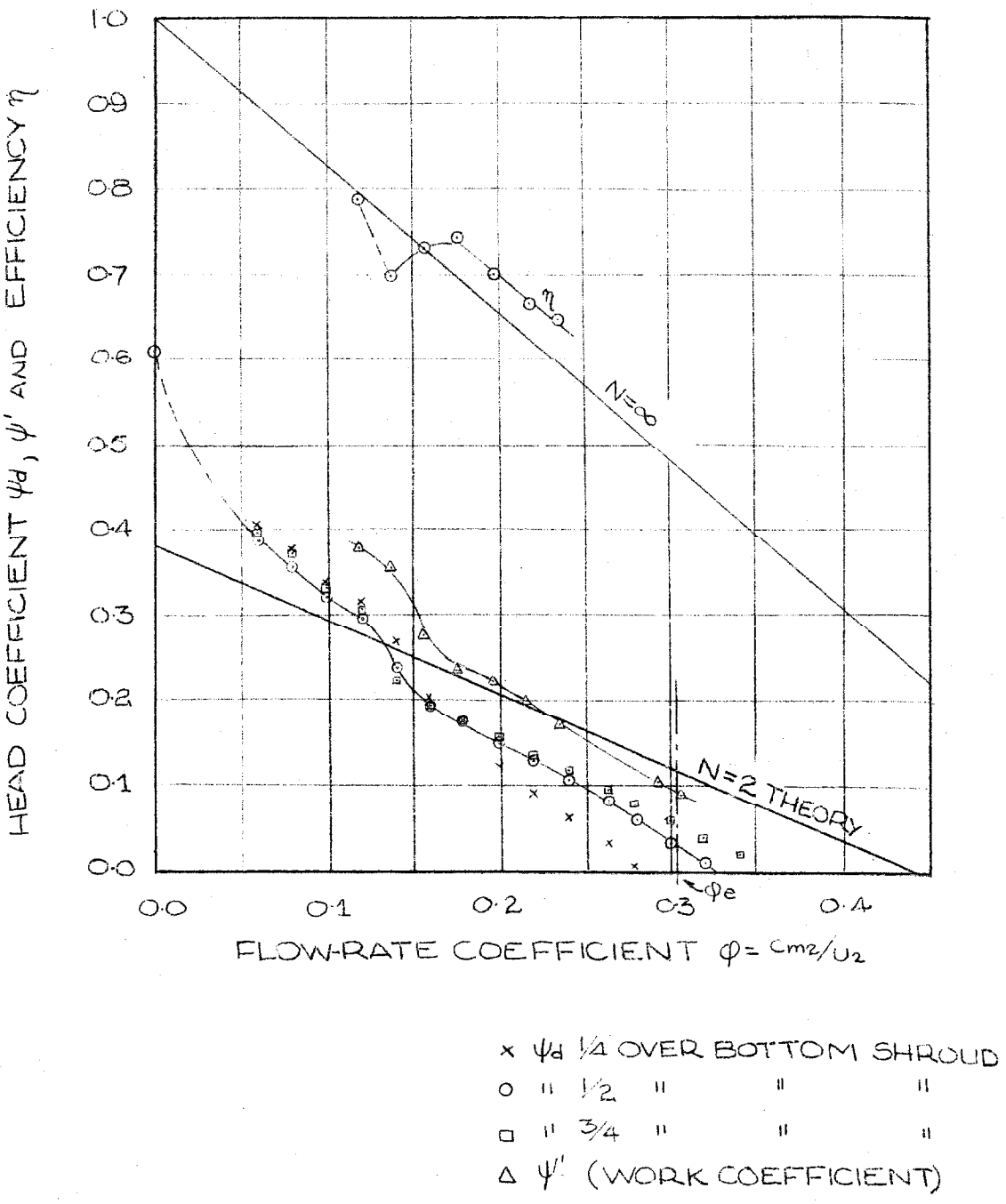

FIG. 14. EXPERIMENTAL AND THEORETICAL HEAD VS. FLOW-RATE CHARACTERISTICS. TWO VANES, $\beta = 30°$, $r_1/r_2 = 0.54$.

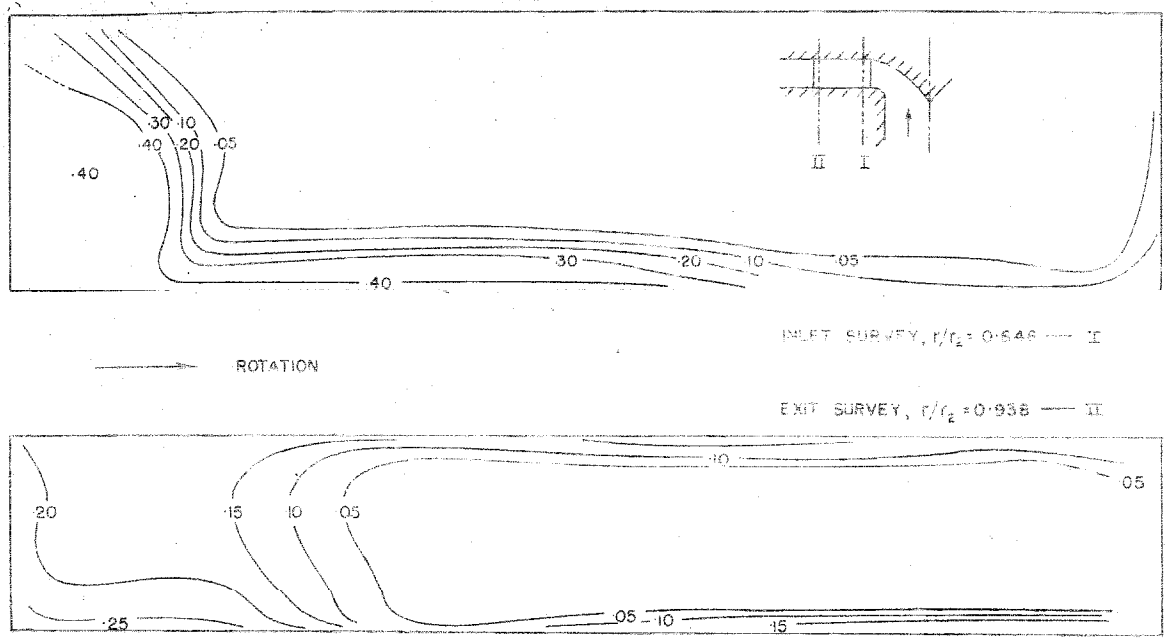

Fig. 15. Contour plots of loss coefficient ζ_r. Six vanes, $\varphi = 0.238$. Developed head = $0.50\ (u_2^2/2g)$. Plotted on the developed passage perimeter which is taken as unity in each case.

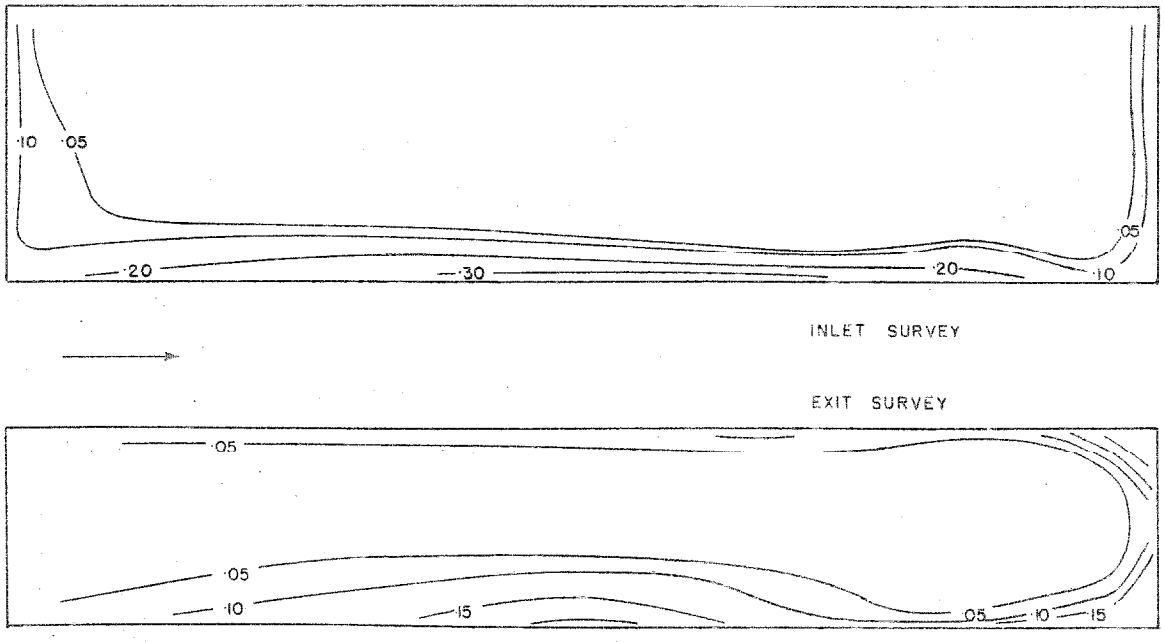

Fig. 16. Contour plots of loss coefficient ζ_r. Six vanes, $\varphi = 0.198$. Developed head = $0.70\ (u_2^2/2g)$.

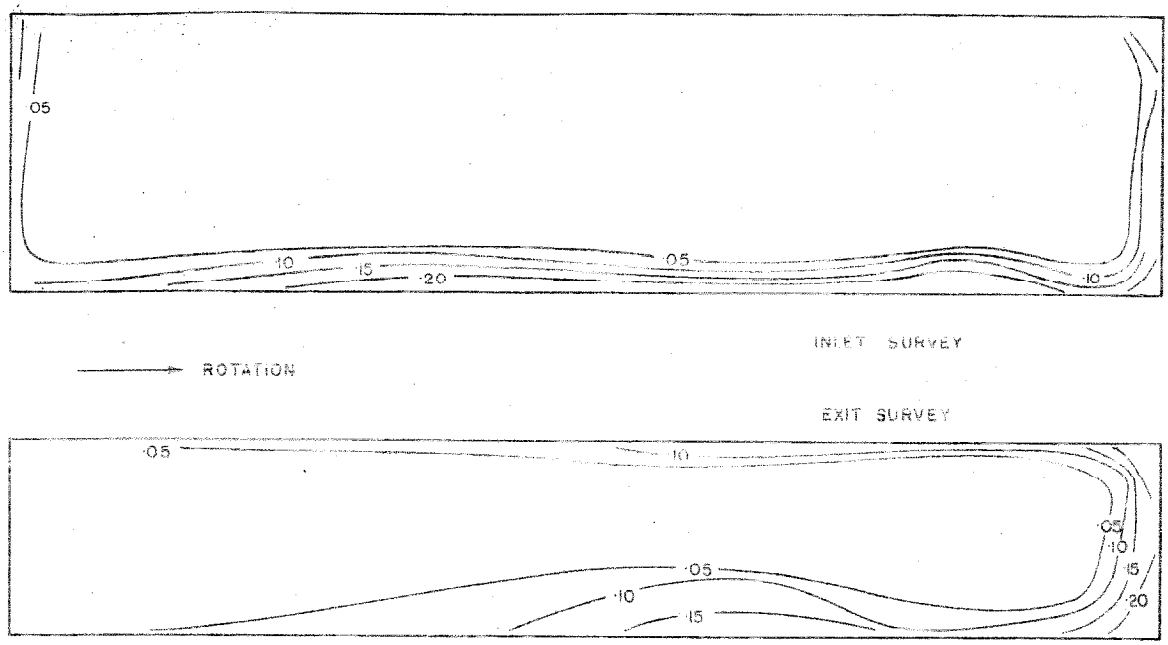

Fig. 17. Contour plots of loss coefficient ζ_r. Six vanes, $\varphi = 0.178$. Developed head = $0.80\ (u_2^2/2g)$.

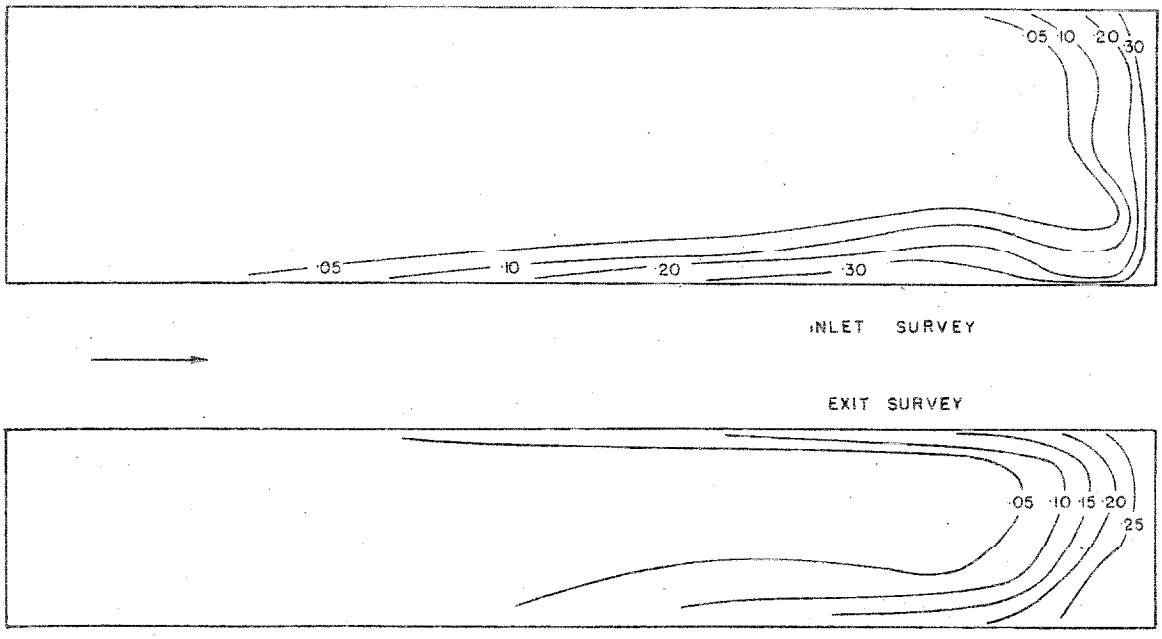

Fig. 18. Contour plots of loss coefficient ζ_r. Six vanes, $\varphi = 0.140$. Developed head = $0.93\ (u_2^2/2g)$.

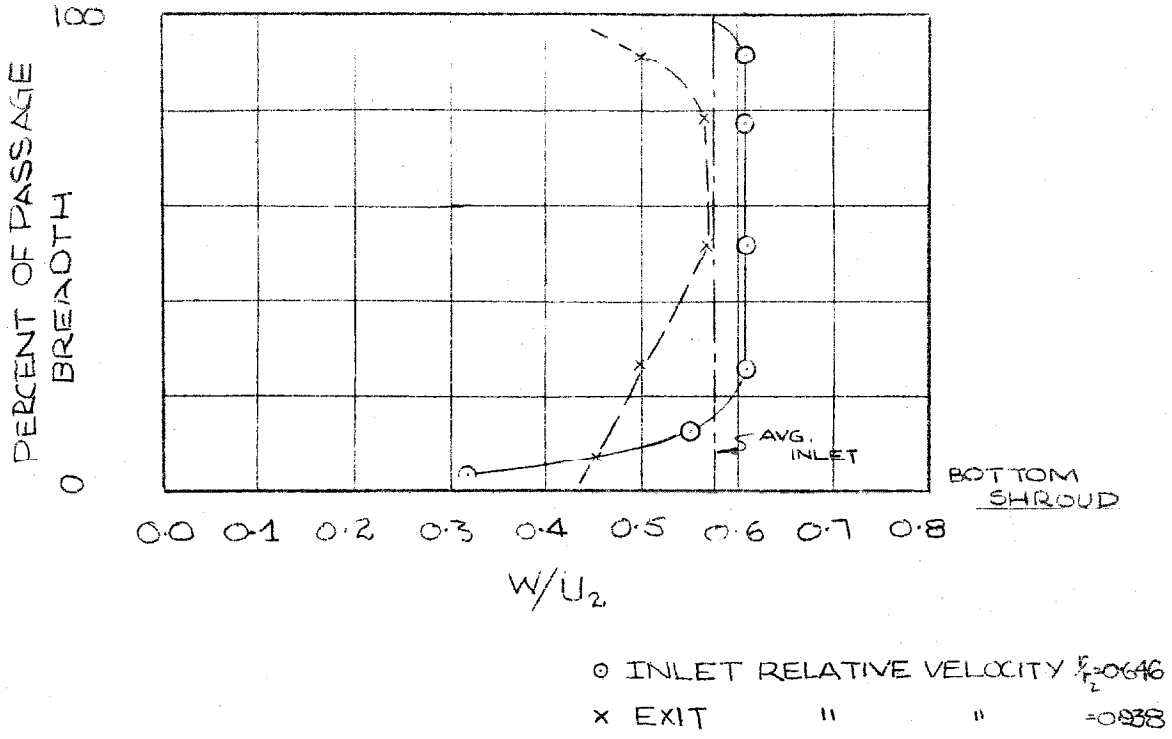

FIG. 19. INLET AND EXIT RELATIVE VELOCITY TRAVERSE ACROSS PASSAGE BREADTH MID-WAY BETWEEN VANES. $\varphi = 0.178$, $N = 6$

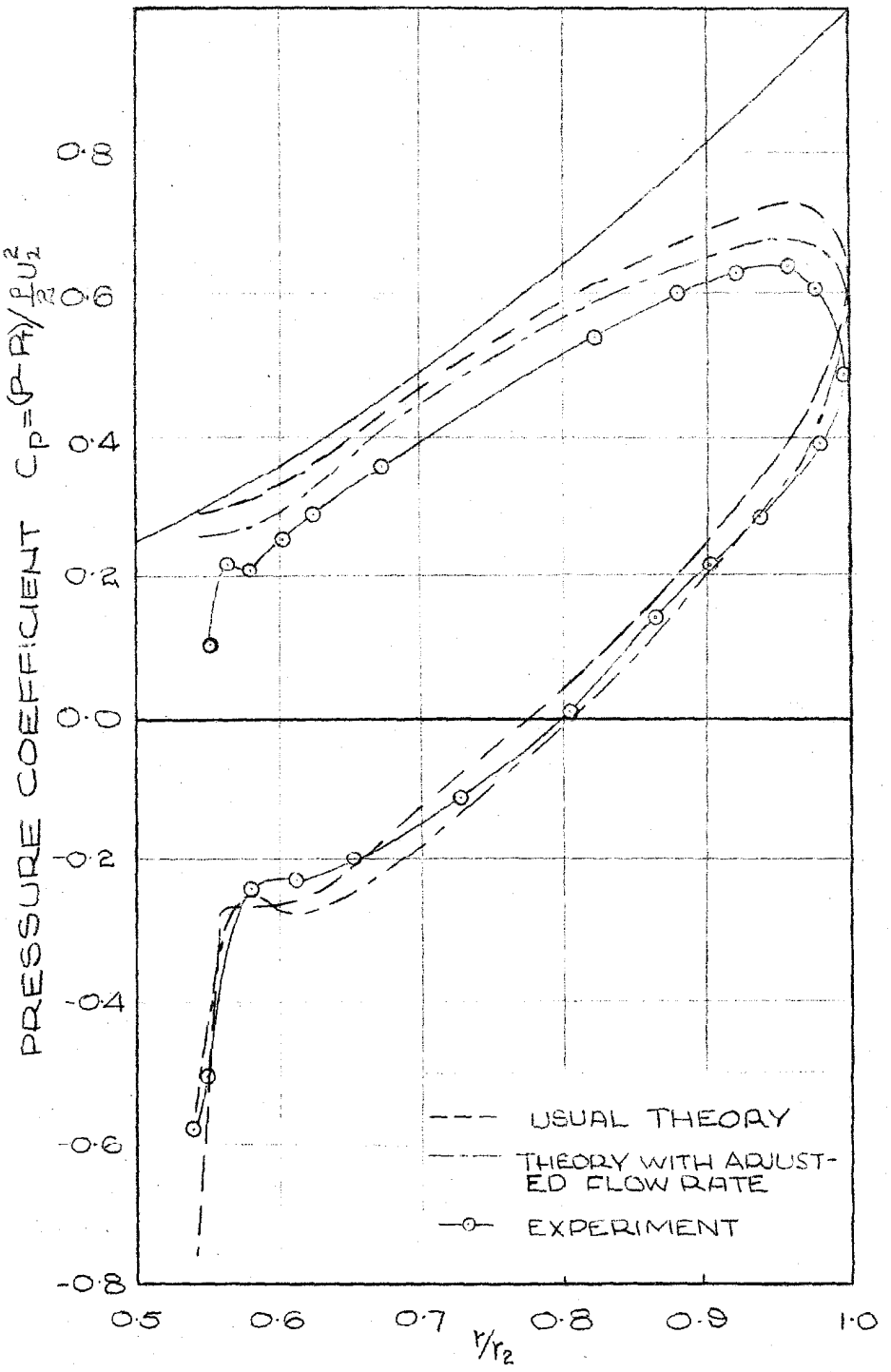

FIG. 20. EFFECT OF MODIFYING FLOW RATE
$\varphi=0.178$, $N=6$

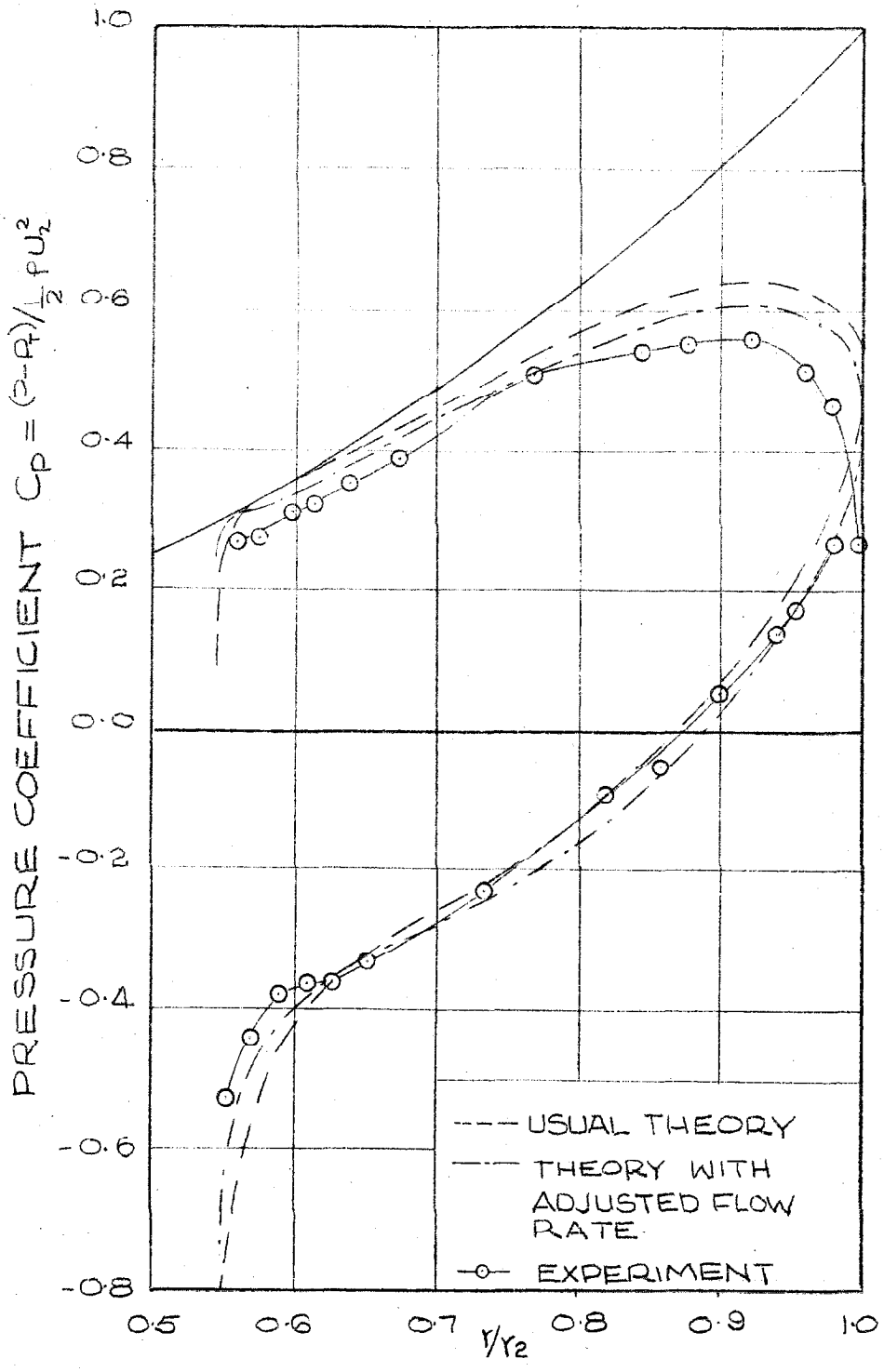

FIG. 21. EFFECT OF MODIFYING FLOW RATE
$\varphi = 0.18$, $N = 4$